University of South Bohemia

Faculty of Science

Assembly of the unique *Trypanosoma brucei* F_1-ATP synthase

Bachelor Thesis

Vladyslav Lazebnyk

Supervisor: RNDr. Alena Panicucci Zíková, PhD

Co-Supervisor: Brian Panicucci

České Budějovice, 2021

Lazebnyk V., 2021: Assembly of the unique *Trypanosoma brucei* F_1-ATP synthase. Bc. Thesis, in English - 64 p., Faculty of Science, University of South Bohemia, České Budějovice, Czech Republic.

Annotation

The catalytic F_1-ATP synthase of the human pathogen *T. brucei* has several unique features. This essential enzyme contains three copies of the novel subunit p18 and it incorporates both subunit α peptides generated by a rare proteolytic event. Therefore, we characterized genetic cell lines that deplete the only two known F_1-ATP synthase assembly factors in order to gain more insight into the fascinating assembly of this parasitic enzyme.

Affirmation

I declare that I am the author of this qualification thesis and that in writing it I have used the sources and literature displayed in the list of used sources only

České Budějovice …….. ……

Vladyslav Lazebnyk

Acknowledgement

I would like to express my gratitude towards my supervisors Brian Panicucci and Alena Zíková, who were always helpful throughout the whole project, guiding me through the challenging, but at the same time extremely interesting world of science. Despite the Covid-19 pandemic, I could always count on Brian`s prompt replies and his assistance. He always supported me with great study materials and his accumulated experience in closely related fields of study. An aspiring researcher can only dream of having such a wonderful mentor!

I also would like to thank the whole team of PARU II lab for their incredible hospitality and for letting me work with them side by side as a real scientist.

Abbreviations

BF – bloodstream form

BN – Blue Native

BN-WB – Blue Native Western Blot

cDNA – complementary DNA

dsRNA – double stranded RNA

ETC – electron transport chain

IND – induced culture

LB – lysogeny broth

MCS – multiple cloning site

mt – mitochondrial

NON – noninduced culture

ORF – open reading frame

OXPHOS – oxidative phosphorylation

PF – procyclic form

qPCR – quantitative polymerase chain reaction

RISC – RNA-induced silencing complex

RNAi – RNA interference

SDS – sodium dodecyl sulfate

ssRNA – single stranded RNA

WB – Western Blot

Table of contents

1. Introduction

1.1 General characteristics of *T. brucei* life cycles

T. brucei is a protist parasitic species belonging to the genus *Trypanosoma*, phylum *Euglenozoa*, reaching up to 50 μm in length [1]. It has an elongated body with a streamlined and pointed shape (Figure 1). These species cause a number of serious blood diseases in vertebrate animals including humans, which can be lethal if not treated. For instance, infected *T. brucei* people suffer from African trypanosomiasis or so-called sleeping sickness – the disease with severe symptoms and neurological disorders. The disease is usually transmitted via bite of infected tsetse fly in Saharan Africa region.

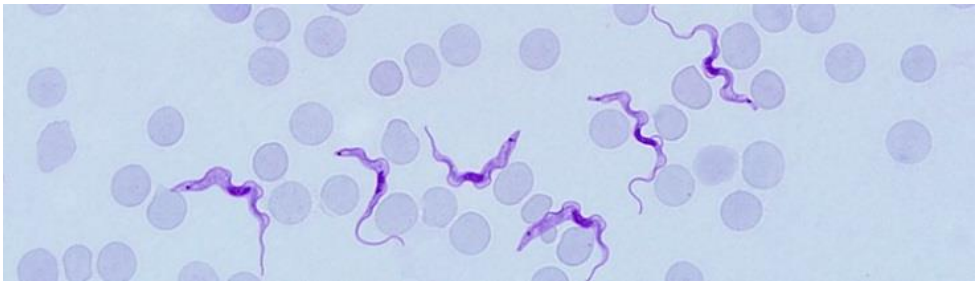

Figure 1: *T. brucei rhodesiense* in a Giemsa-stained blood smear (*Centers for disease control and prevention*).

While living inside the insect (procyclic form - PF) or mammalian (bloodform - BF) host, the *T. brucei* parasite can undergo few metamorphosis throughout its complex life cycle, thus adjusting to the current living environment (Figure 2).

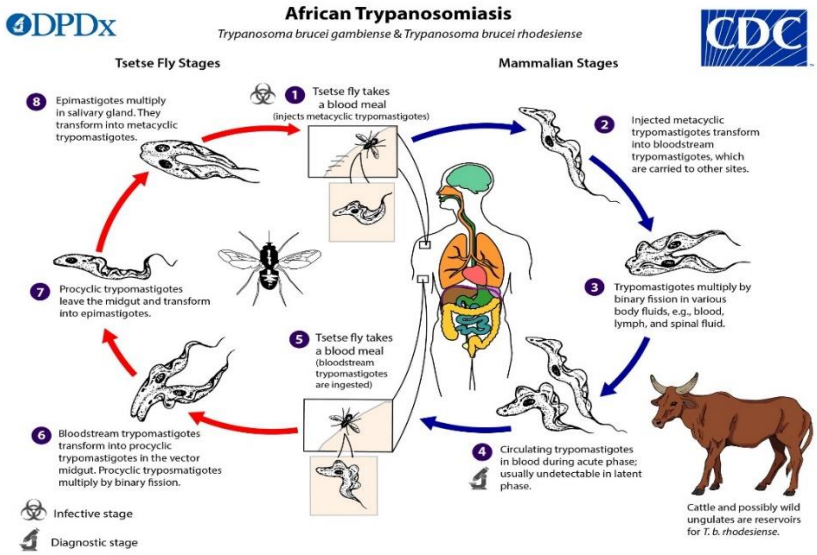

Figure 2: Procyclic and bloodstream life cycles of *T. brucei* (*Centers for disease control and prevention*).

Bloodstream forms are peculiar for the presence of variant surface glycoproteins (VSG) on the cell membrane (pellicle) of the parasites. VSG are densely packed on the surface of the membrane, which enables them to evade the mammalian host`s immune system, leading to the development of

chronic diseases. Notably, bloodform *T. brucei* are one of the few species known to pass the blood brain barrier, which makes them even more dangerous pathogens [2]. Likewise, bloodforms differ morphologically from the procyclic ones – they are generally smaller and more mobile. Although, both forms share a remarkable feature – a network of large circular mitochondrial DNA called kinetoplast (also referred as kDNA), usually located at the surface of the flagellar basal body, in the tripartite attachment complex. This concatenated DNA is believed to play an important role in encoding some subunits of the mitochondrial ribosome and complex enzymes involved in oxidative phosphorylation.

The different environments provided by the insect vector or the mammalian host means that the parasite must utilize various carbon sources to produce energy in the form of ATP. For instance, PF cells primarily utilize proline to produce reducing reagents that provide electrons for the electron transport chain, while BF do not use ETC at all [3]. BF parasites lack cytochrome c and therefore they do not possess functional ETC complexes III or IV to pump protons outside the mitochondrial membrane. Instead of using the proton-gradient motive force to create the ATP during OXPHOS, BF cells rely on the special organelle called the glycosome, which house the enzymes required for glycolysis. Since BF parasites encounter excess levels of glucose in the blood, it is sufficient and preferable to just utilize glycolysis to generate 2 net ATP per 1 molecule of glucose [4]. However, mitochondria in BF parasites is still involved in variety of vital processes. For instance, it take part in the Fe-S clusters assembly – ubiquitous cofactors of proteins, which are essential for the cell functioning [5]. Since these proteins encode in the nucleus of the cell, BF mitochondria have to keep a membrane potential for the protein import. In such scenario, the F_OF_1-ATP synthase hydrolyzes ATP and rotates in reverse orientation, in order to pump protons into the mitochondrial inner membrane space. This activity of the enzyme is essential in the BF parasite.

1.2 Energy metabolism and oxidative phosphorylation in PF *T. brucei*

T. brucei is the unicellular eukaryotic organism and the PF of the parasite maintains typical metabolic pathways. However, mechanisms of regulation of mitochondrial metabolism in *Trypanosomes* are not yet fully understood [3]. For example, Coustou V. (2003) states that level of intracellular ATP concentration did not decrease dramatically in case of F_0F_1-ATP synthase oligomycin inhibition, and the doubling time of the parasite was only 1.5-fold increased with a 10-fold excess of antibiotic. In contrast, the cytosolic pyruvate kinase knockout (PYK) by RNAi – the enzyme responsible for pyruvate synthesis, led to the high mortality rate of the cells, which indicates that the cytosolic substrate level phosphorylation might be essential for the PF parasites [6]. On the other hand, according to Huang G. (2013), mitochondrial calcium uniporter (TbMCU) is crucial for the regulation of mitochondrial bioenergetics in *T. brucei,* marking a great growth defect in case of its depletion for both PF and BF parasites [3].

Nevertheless, the main pathway for ATP production for PF *T. brucei* is through oxidative phosphorylation with proline as the main energy source. In this case, energy metabolism operates in its classical way, transforming the mechanical work of ATP-synthase into chemical energy in a form of ATP molecules (Figure 3).

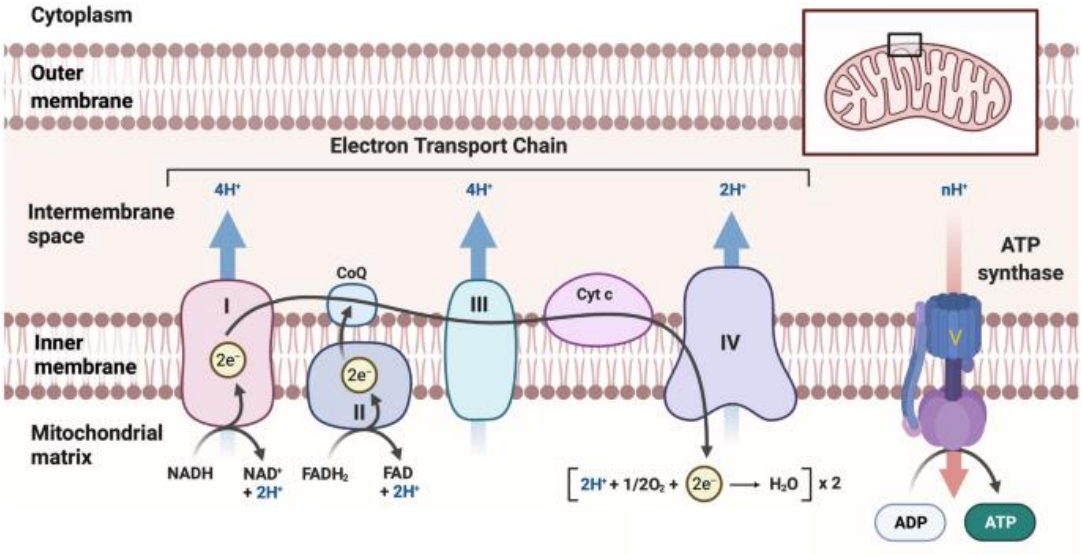

Figure 3: Process of oxidative phosphorylation including ETC *(Generated using BioRender)*

A group of enzyme complexes (from I to IV) is located on the inner membrane of the mitochondria, which together with the two auxiliary complexes ubiquinol (CoQ) and cytochrome C, form the electron transport chain (ETC). As known, ubiquinol is a fat-soluble coenzyme, while cytochrome C is a heme protein [7]. These two complexes pass electrons through the ETC to the terminal electron acceptor – O_2, which in the end forms 2 molecules of water. In addition, the essential cofactors NADH and $FADH_2$ are generated in the Krebs cycle and then are oxidized by complex I (ubiquinone oxidoreductase) and complex II (succinate dehydrogenase) respectively. These cofactors thus donate their electrons to the ETC as it is illustrated on the representative image (Figure 3). Electrons are then transferred from reduced ubiquinone to complex III (cytochrome C oxidoreductase), which passes them further to complex IV (cytochrome C oxidase) via the cytochrome C electron-carrier.

This electron relay allows protein complexes I, III and IV to pump protons into the inner membrane space, thus creating an electrochemical gradient. In the end, the potential energy of the proton motive force is utilized by the F_OF_1-ATP-synthase complex (complex V) to generate ATP molecules. The rotary part of the ATP synthase turns under the force of proton flow, causing conformational changes in the stationary part, which then mechanically binds ADP and inorganic phosphate (Pi) molecules together in its catalytic sites.

1.3 Function and structure of ATP-synthase

The overall structure of the eukaryotic ATP-synthase is highly conserved among species of life. Generally, ATP synthase resembles a 'watermill' or unusually efficient biological rotary motor, which converts potential energy into physical energy. This sophisticated multisubunit molecular machine consist of 2 main subcomplexes – catalytic F_1 and membrane embedded F_0 domains (Figure 4). The F_0 subunit consists of the peripheral (stator) stalk, supernumerary proteins and depending on a species [8], up to 15 identical c-subunits (ATP9 molecules) that form the membrane embedded c-ring. Excess protons from the intermembrane space are allowed to flow through the proton channel formed by the c-ring and subunit *a*. The flow of protons causes the rotation of the c-ring, which in turn drives the γ-subunit of the central stalk of the enzyme. Since the asymmetrical structure γ-subunit is immersed into the head of the F_1 domain, its rotation causes conformational changes in the hexameric ring of the F_1 module. This hexameric ring is comprised of three alternating copies of the α and β subunits, which form the catalytic head of the F_1 domain. In eukaryotes, the F_1 domain protrudes into the mitochondrial matrix, but it is held in place by the peripheral stalk [9].

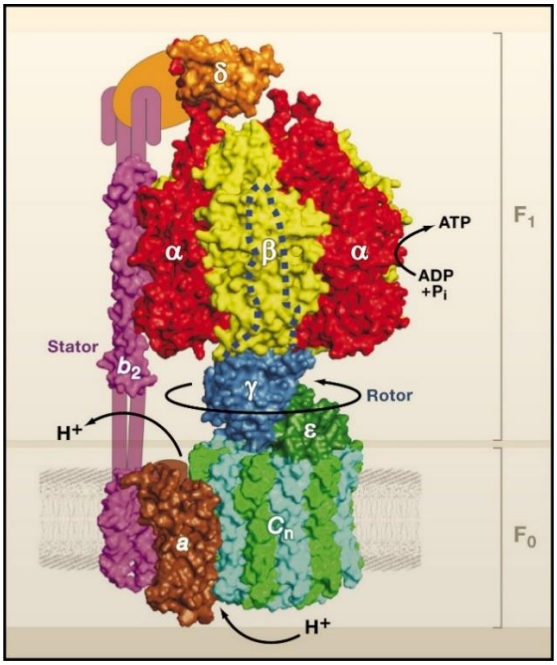

Figure 4: Structure of F_0F_1-ATP synthase. Protons enter the c-ring shown in light-blue and light-green in the F_0-module (1 proton per each c-subunit) and cross the mt membrane through the proton pore in the subunit a, shown in brown. This interaction causes the rotation of γ, (shown in blue) since it is attached to the c-ring, by the principle of gear wheels. This led to the conformational changes in the $\alpha_3\beta_3\delta$-catalytical head (red, yellow, light-brown respectively), which in turn allows to generate ATP-molecule from ADP and Pi. Peripheral stalk shown in purple holds 2 modules and other subunits together and additionally prevents the unwanted rotation of $\alpha_3\beta_3$-hexamer [8, 9]. (*Weber J., (2006). ATP synthase: subunit-subunit interactions in the stator stalk*).

According to Moran L. (2007), for every three protons which enter the matrix through the pore, the rotor moves approximately 120°, so it takes 9 protons to complete one full rotation [10]. The γ rod is asymmetric and as it rotates inside the F_1 module, the peripheral stalk keeps the α-β head group in place, which causes the conformational changes that provide the catalytic energy needed to

generate ATP. Depending on its orientation, each β-subunit can be present in one of three different states: loose, open and tight (Figure 5). When a given subunit is in the open state, ADP and phosphate bind to its catalytic site. In the second, or the loose state, ADP and Pi are secured in place and cannot be released. Upon rotation β-subunit changes its conformation once again, this time to the tight state [11]. Here ADP and Pi are linked together due to the energy provided by the mechanical force and released afterwards as the ATP molecule. This principle was first described by Paul D. Boyer and his colleagues in 1982 after a series of X-ray crystallographic studies and experiments using ^{18}O-labeled isotopomers of P_i, for which his team received a Nobel Prize in 1997 [12].

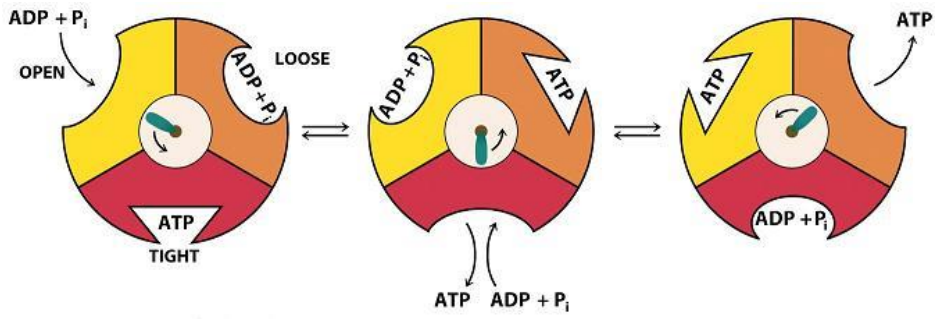

Figure 5: The binding change mechanism. Schematic showing the three different catalytic states of β-subunit – open (arc), loose (ellipse) and tight (triangle). The γ-subunit is illustrated in the middle as the spinning rod (*Moran L., Horton R., Scrimgeour G., et al. (1994) Principles of Biochemistry 4th edition*).

1.4 Assembly of F_0F_1-ATP synthase

ATP synthase *in vivo* is not a self-assembling enzyme. This is much more sophisticated molecular complex, consisting of numbers of different protein subunits, with a total molecular weight of over 500 kDa [13]. For instance, human mt ATP synthase is comprised of 29 subunits, which together organize the membrane-extrinsic (F_1) and membrane-intrinsic (F_0) domains [14]. Therefore, under normal growth conditions, the assembly of such a complex requires the assistance of specialized chaperone proteins, also known as assembly factors, in a continuous step-by-step process.

To date, the assembly of the yeast ATP-synthase has been studied the most extensively [14, 15]. Despite the fact that the overall structure and functions of ATP synthase are highly conserved among species, phylogenomic studies have shown significant discrepancies between mammalian, protozoan, bacterial (cell wall) and plant (chloroplast) assembly factors of the enzyme. Some of them have different chemical structure or enzymatic activity, while some are even absent in one or another organism, which in turn changes some of the key steps in the assembly process itself [8]. Here, we mainly describe the yeast ATP synthase assembly, as it is a model organism.

Recent studies reveal that the assembly of the whole ATP synthase enzyme begins from several pre-constructed subcomplexes in a strictly determined order, involving formation of several defined intermediates. This order is characterized by the branched pathway, where assembling of different subunits and/or intermediates occurs independently of each other. Thus, the F_1 domain, the $\alpha_3\beta_3$

hexamer and the central stalk γδε are formed independently of both F_0 and the stator module. The pore-forming complex, consisting of the c-ring and subunit *a*, is assembled last, in order to protect the mitochondria from an energy-wasteful proton leak and the consequent dissipation of the mitochondrial membrane potential [8, 16].

Biogenesis of the ATP synthase also requires well-coordinated and balanced expression of gene products of the enzyme subcomplexes, since they are encoded in two physically distinct genomes – mitochondrial and nuclear [14, 16, 17]. According to Tzagoloff (1969), wild type yeast grown in the presence of chloramphenicol, an inhibitor of mitochondrial translation, were still able to synthesize the F_1-module. This demostrates the independence of the assembly process since the mitochondrial encoded subunits are strictly found in the F_O-ATP synthase. This also illustrates the presence of an elaborate regulatory mechanism that maintains the correct stoichiometry of the intermediates [18]. Remarkably, most of the polypeptides and auxiliary subunits are nuclear encoded and transferred into the mitochondrial matrix, and only three of them – ATP6, ATP8, and ATP9 are part of the membrane F_0 domain [16].

Assembly of α and β subunits in the F_1-domain is promoted by the binding of ATP12 and ATP11 chaperones respectively (Figure 6), which prevents the formation of unwanted high-molecular weight insoluble α-α, β-β homomeric aggregates [8, 16]. It was suggested that these chaperones replace constituent α and β subunits during the assembling of the hexameric barrel, due to their similar chemical structure. Furthermore, they keep the noncatalytic and catalytic site interfaces between them occupied, preventing concomitant detrimental interactions in the immature complex [19].

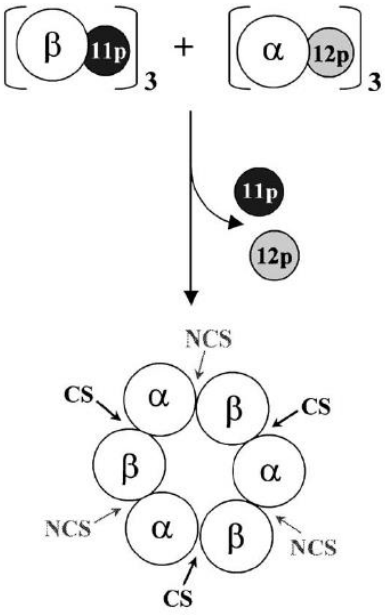

Figure 6: ATP11, ATP12-mediated F_1 assembly. CS – catalytic site; NCS – noncatalytic site (*Ackerman S.H., (2002). Atp11p & Atp12p chaperone F_1 ATPase biogenesis*).

Some of these statements, however, have been clarified and to date, it is believed that γ-subunit appears responsible for the initiation of α and β release from their assembly factors. This is because of the significantly similar structure of its peripheral coiled-coil tail to the C-terminal helical fragment of ATP12, which was found to be crucial for its activity [20]. Other chaperones, Fmc1p (found only in yeast) and Hsp90, are necessary for proper F_1 assembly in case of high temperature stress [8, 13]. Notably, increased levels of the ATP12 assembly factor can compensate for the absence of Fmc1p, which could mean that Fmc1p has a folding but not the structural function [21].

The first step in the F_0-module assembly is the oligomerization of ATP9 subunits (subunit *c*) into a hydrophobic c-ring, which, as previously described, occurs independently of other components. ATP25, Aep1p and Aep2p are nuclear encoded ancillary factors, required for proper ring formation. Notably, ATP25 is post translationally cleaved into two polypeptides of a 32 kDa, which is responsible for ATP9 mRNA stabilization, and a 35 kDa, which directly participate in the assembly of the c-ring [8, 16]. Once the c-ring is formed, it is suggested that the F_1-module binds it via the central stalk subunits γ, δ and ε, constituting a large ATP-synthase intermediate (Figure 7).

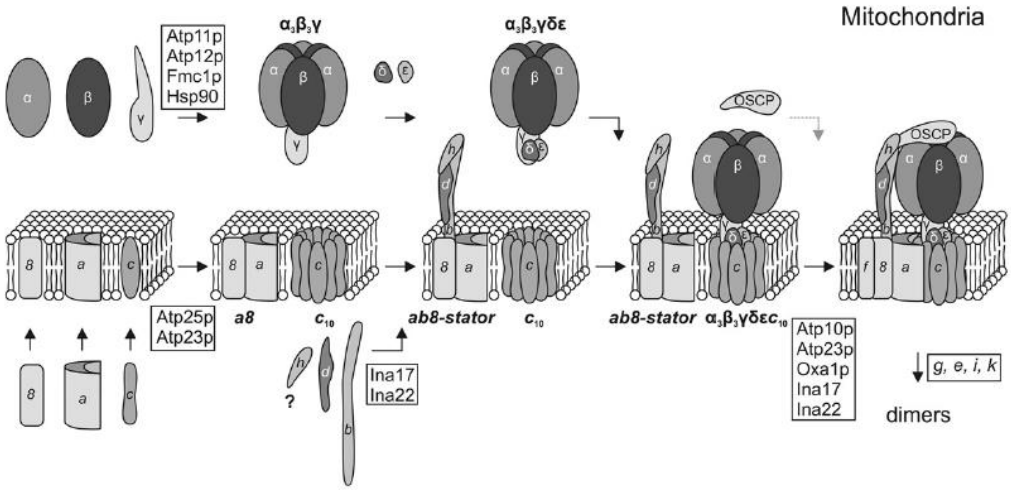

Figure 7: Detailed ATP-synthase assembling process. The graph represents independent formation of transient intermediates in the different parts (modules) of the enzyme from a single subunits (shown with the corresponding names), which associate together with the help of a special assembling factor proteins (shown in squares), and in the end create mature ATP-synthase complex in mitochondria cristae *(Rühle T., Leister D., (2015). Assembly of F_1F_0-ATP synthases).*

Another crucial factor is the ATP10 assembly protein, which creates a physical complex with the membrane-embedded components of the peripheral stalk – ATP6 and ATP8 (subunits *a* and 8 respectively). This transient complex is often times believed to be a third module in the assembly process since it represents another independent intermediate that facilitates the consequent association of the ATP6/ATP8-containing module with the maturate c-ring. This in turn creates a core for further proton pore formation [8]. Remarkably, this complex additionally comprises ATP23, a metalloprotease that removes first ten amino acids at the N-terminal region of the ATP6 precursor

during its post-translational maturation. However, experiments with mutant yeast strains reveal that beside its proteolytic activity, ATP23 is also directly required for the interaction of the c-ring and the peripheral stalk intermediate, implying that some of the ATP10 and ATP23 functions are overlapping [16, 22]. Oxa1p translocase is needed for proper assembly of ATP6 with the c-ring, as well as for the membrane insertion of several imported proteins into the mitochondria. Linkage of F_0 and F_1 modules together with the peripheral stalk in the last step of ATP-synthase formation is promoted by the inner membrane complex INAC, which is composed of the two proteins Ina22 and Ina17 [8, 16].

Eventually, the completely assembled ATP-synthase monomer interacts with the neighboring one via the *b* subunits membrane-spanning segments that are mirrored towards each other. Subunits *e, g, k* and *i* are also involved in the dimer formation, which mediate the stabilization of its final structure. Dimerization of ATP-synthase in yeast occurs at the angle of 86º so two adjacent monomers resemble a V-shaped nexus. This specific angle determines the unique curved shape of the mitochondrial inner membrane and allows ATP synthase dimers to fold into the rows, which in turn ensures the most effective ATP production during energy metabolism [8].

1.5 Unique factors of *T. brucei* ATP synthase

As it was mentioned before, despite the common origin of F_0F_1-ATP synthase and the general resemblance of its structure and function among organisms, some of characteristics have dramatically changed over the course of evolution and eventually became unique features in some species. Hence, in *T. brucei*, a member of the *Euglenozoa* phylum, a number of novel proteins were recently discovered that appear to be crucial for the structural integrity of the ATP synthase and for the regulation of its energy metabolism overall [23]. Some of them may have substituted homologous subunits found in other eukaryotic organisms, but some had no recognizable counterparts in any species, being potentially connected with a specific parasitic life cycle [24].

One such striking *T. brucei* protein is the pentatricopeptide repeat subunit p18, which is associated with the external surface of the α-subunits in the F_1 catalytical domain (Figure 8). This protein is present in three copies per each ATP synthase complex, but more interestingly, it is found in both procyclic and bloodstream forms of the parasite, which suggests an idea that it is not necessarily parasite-specific factor, but rather has some assembly function and was developed in a deviated branch of evolution [25, 26]. This hypothesis is supported by the fact that atypical p18 subunit was also found in some other *Euglenozoan* species, for instance in *Euglena gracilis*, – a common freshwater inhabitant, which does not have a parasitic lifestyle [27]. To date the exact role of p18 still remains obscure, but it is undoubtedly essential for the proper functioning of ATP synthase enzyme [26]. According to Gahura (2017), in the PF and BF *T. brucei* cells, whose p18 expression was suppressed by RNAi, levels of F_1-ATP synthase were decreased dramatically [25].

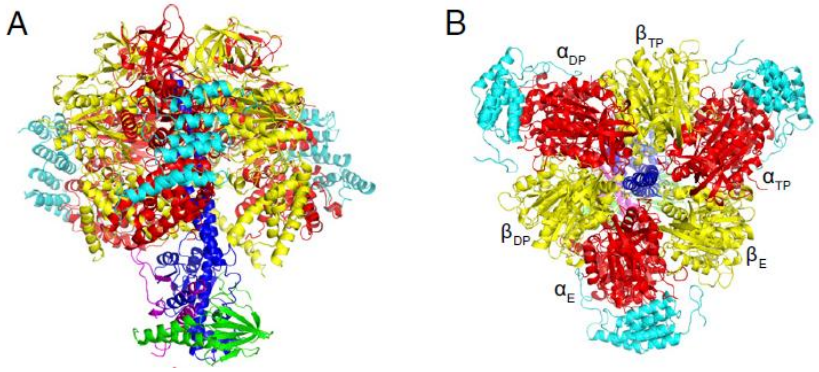

Figure 8: Association of p18 protein (light-blue) with α-subunits (red) in F_1 ATP-synthase domain. Other constitutive subunits β, γ and δ are shown in yellow, blue and green respectively. (*Montgomery M.G., Gahura O., Leslie G.W., et al, (2018) ATP-synthase from Trypanosoma brucei has an elaborated canonical F_1-domain and conventional catalytic sites*).

Another remarkable feature is that the α-subunit in *T. brucei* is proteolytically cleaved at two sites, forming an N-terminal and C-terminal α peptides with molecular weights of 13 and 47 kDa. Currently, there is no information about the purpose of this cleavage or how exactly it affects the ATP synthase assembly. Furthermore, it is also not well known whether this cleavage happens before the complex is assembled or after, but presumably this process is biologically significant [25]. It is also not fully understood how the parasite assembles these unique proteins together. Does p18 help in the assembly of the C-terminal α peptide or is there some other, yet undiscovered assembly factors.

All of the aforementioned features, such as unique metabolic pathways and atypical structure of protein complexes with essential functions are attractive drug targets from the pharmacological perspective. Nowadays, available drug therapy against *Trypanosoma* parasites that are responsible for several severe human and livestock diseases, have a lot of serious side-effects. Furthermore, drug resistance is gradually increasing. On the other hand, these unique characteristics are highly valuable from the evolutionary point of view. They might represent a major step towards deciphering previously not fully investigated properties of the respiratory chain of both an early diverged eukaryote and a lethal human parasite [23]. Therein lies the *significance* of this study.

Therefore, the most important *aims* of this work are as follows:

- To investigate whether PF *T. brucei* ATP11 & ATP12 auxiliary factors are essential for F_oF_1-ATP synthase assembly, by RNA interference
- To examine how the depletion of ATP11 & ATP12 affects the stability of other F_1-ATP synthase subunits
- To determine if the loss of ATP11 or ATP12 produces any subcomplexes that might provide insight about F_1-ATP synthase assembly

2. Materials and Methods

2.1. Cell cultures

The experiments outlined in my thesis required the use of a *Trypanosoma brucei* cell line capable of regulatable RNA interference (RNAi). Therefore, we used a PF 427 *T. brucei* cell line genetically modified with the pSMOX plasmid, which we abbreviate as PF Tb pSMOX. The pSMOX plasmid encodes for the heterologous expression of constitutively expressed T7 RNA polymerase and Tetracycline repressor (TetR). These two proteins will only interact with specific DNA elements engineered into an RNAi plasmid. RNA transcription initiation of the integrated interfering RNA fragment occurs at the upstream T7 RNA Pol-promoter sequence. However, the polymerase is physically impeded by the binding of the TetR to the Tet-operator, positioned immediately downstream of the promoter. Upon the addition of tetracycline to the media, the TetR changes conformation and is no longer capable of binding the Tet-operon, allowing the RNA polymerase to proceed with transcription (Figure 9). This plasmid also contained genes for puromycin resistance, which was used as a selectable marker.

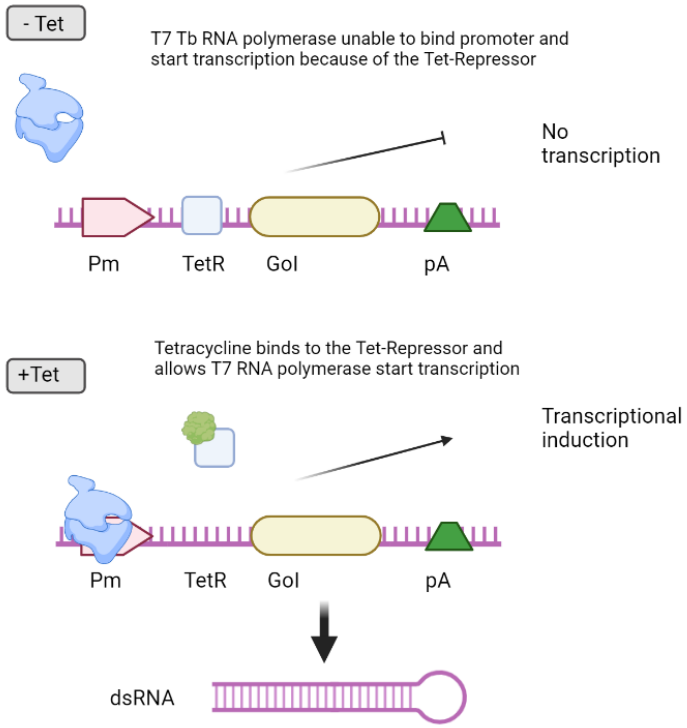

Figure 9: Tet-On RNAi system. Tetracycline binds to the Tet-repressor and causes a conformational change that allows the T7 polymerase to transcribe the downstream gene and create a double stranded RNA fragment (*generated using BioRender*).

For regular maintenance of the cell lines, the parasite cultures were grown at 27 °C in 25 cm^2 plastic flasks with 10 ml of SDM-79 medium, prepared from premixed powder (Table 1). When higher cell numbers were needed, they were transferred to 75 cm^2 flasks with the capacity of around 50 ml of the culture.

Table 1: SDM-79 medium + 10% FBS

Reagent	5 L
MilliQ	861.5 ml
Premixed SDM-79 powder	25.5 g
Pen/Strep (10^4U/ml), 100x	10 ml
Hemin (2.5mg/ml)	3 ml
FBS	100 ml
Phleomycin	1 µl
Puromycin	1 µl
Adjust pH to 7.3 with 10M NaOH	

Puromycin was added to the medium to maintain the drug selection of PF Tb pSMOX cell lines. In case of PF Tb pSMOX RNAi a mixture of puromycin and phleomycin antibiotics were used. A working stocks of 1 mg/ml puromycin and 2.5 mg/ml phleomycin were diluted 1:1000 for a final concentration of 1 ug/ml and 2.5 ug/ml respectively. Trypanosome cells were checked daily under the microscope for their density, motility and morphology to assure that the cells were healthy and not stressed. PF *T. brucei* cells prefer to be kept under fairly dense conditions, between $1x10^6$ – $1x10^7$ cells/ml and can be severely stressed if they are diluted too much or if the density of the culture is above $2\text{-}3x10^7$. Since the doubling time of the cells is approximately 8-9 hours, we normally split a $1x10^7$ cells/ml culture 1:10 with fresh media every other day to keep the steady concentration. In case if a dense culture was needed for the following day, the cells were diluted only 1:3 with fresh media. Cell lines should generally not be maintained for more than 6-8 weeks as this can lead to the selection of mutants that have lost genetic controls introduced into the cell line or have altered metabolism due to extended time in the culture. To prevent the degradation of genetic modifications over time, cell lines could be cryopreserved in liquid N_2. For this, 500 µl of well-grown cells in a late log phase ($1\text{-}2x10^7$ cells/ml for PF) are carefully mixed with 500 µl of freezing solution (Table 2) in special cryovials and placed at 80 ºC for three days. Then, the stabilates are transferred to the liquid nitrogen tank and if needed, can always be thawed back and checked for its viability. This option is one of the critical factors that makes *T. brucei* a great model organism.

Table 2: Stabilate Freezing Solution*

Reagent	FW or [Stock]	[Final]	500ml
MilliQ			200 ml
Glucose	180.16	100 mM	9.3 g
NaCl	58.44	72 mM	2.1 g
Sodium Citrate	294.1	5 mM	0.75 g
BSA	66.78	15 mM	0.5 g
Glycerol	80 %	12 %	75 ml

* – after preparation, solution should be filter sterilized with 0.2 µm filter

2.2. Cell counting

In order to ensure that the cell cultures remain within the mid-log growth phase, the cell density was routinely counted on the 'Z2' Coulter Counter (Beckman). The principle of its work is based on the detection and measurement of changes in electrical resistance produced by a cell suspended in a conductive liquid. The cells, passing through a small aperture, function as discrete insulators, which immediately modulate the impedance of the electrical path between two submerged electrodes located on each side of the aperture. This results in an electrical pulse, suitable for counting and sizing the cell culture [28].

Before counting, the samples were prepared by carefully mixing 100 µl of the Trypanosomatid Cell Fix solution (Table 3) with 100 µl of each cell culture in a 1.5 ml test tube. The formaldehyde present in the solution fixes the proteins of the cell, keeping them intact and making sure the counter does not become contaminated with any pathogens. After thoroughly mixing the cell suspension by pipetting up and down repeatedly, 50 µl of the mixture was introduced to a cuvette containing 5 ml of isotonic Hemosol. The cuvette was then loaded onto a spring-loaded platform and raised to submerge the aperture into the cell suspension. The counting process was initiated when a vacuum was established to move the cell suspension through the aperture. It was previously determined that the most accurate counts occur when the settings of the machine are set up for the particles size between 3.5-7.5 um. This is due to the fact that *T. brucei* is a long slender organism that can pass through the aperture in various orientations, with the extremes being completely vertical or horizontal.

Table 3: Trypanosomatid Cell Fix Solution

Reagent	**[Stock]**	**Amount**	**[Final]**
dH_2O		85 ml	
SSC	20x	5 ml	1x
Formaldehyde	36%	10 ml	3.6%

2.3. Growth curves

Since we are trying to determine the function of the F_0F_1-ATP synthase assembly factors ATP11 and ATP12 in the creating of its unique structure, the first step is to analyze whether these proteins are essential for cell growth. Therefore, we can examine the growth rate of RNAi induced PF pSMOX cultures compared to noninduced. By growing each PF pSMOX RNAi cell line in two flasks, one containing tetracycline to activate the RNAi system and one without, we can observe if the depletion of ATP11 or ATP12 affects the doubling time of the culture. For more coherent values, we calculated the cumulative density of each culture as if it was contained in a flask with limitless volume. The cell density of each culture was measured every 24 hours. To keep the cell densities relatively consistent between conditions (tetracycline induced RNAi and noninduced cells), we calculated the volume of the culture that should remain in the flask to seed $3x10^6$ cells/ml. The remaining culture was discarded

and replaced with an equal volume of fresh media to maintain the total culture volume at 10 ml. This media contained the appropriate antibiotics for selection and RNAi regulation. The amount of cells retained in the flask was then used to calculate the dilution factor for that day. The cumulative dilution factor could then be tallied throughout the growth curve by multiplying the current dilution factor with the previous dilutions. Finally, the cumulative cell density was calculated by multiplying the daily density by the running cumulative dilution factor. After ten days, these values were graphed to visually determine if the culture depleted of one of the assembly factors increased the doubling time.

2.4. Real-time quantitative PCR

2.4.1 Quantitative PCR overview

To verify the effectiveness of ATP11 & 12 RNAi depletion, real-time PCR (qPCR) was performed. Since we have not synthesized antibodies to recognize these two gene products yet, we determined the efficiency of the RNAi to deplete the targeted transcripts. qPCR measures the amount of a specific RNA in a population of cells by treating isolated RNA to generate cDNA that provides the template for a quantitative PCR reaction using a special fluorescent dye SYBR Green^{TM}, that binds to the double-stranded DNA. A thermocycler, coupled with fluorometer, modulates the reaction temperature during DNA amplification, while also monitoring the fluorescence signal at each PCR cycle, generating a real-time qPCR curve. The main working principle is that the dye fluoresces when bound to dsDNA but displays weak signal in a presence of a ssDNA. This results in an increased fluorescence as the reaction progresses and dsDNA is formed. When the signal is strong enough, we can determine a quantification cycle, or Cq value. This value can then be used to estimate relative target abundance between different samples.

2.4.2 RNA isolation

First, we isolated RNA from $1x10^8$ *T. brucei* using the RNeasy mini kit that utilizes spin columns (Qiagen). Our samples for qPCR analysis included both noninduced RNAi cells, as well as *T. brucei* induced with tetracycline for 2 or 4 days. The suspended parasites growing in TC flasks were harvested by centrifugation at room temperature for 10 minutes at 1300 xg. After thoroughly removing all traces of media, the cell pellet was resuspended in a buffer that lysed the cells to release all nucleic acids. Ethanol was added to the lysate to aid the binding of RNA to the membrane in the spin column. The membrane was then treated with a series of wash buffers to remove cellular contaminants and high concentrations of salt from the lysis buffer. The bound RNA on the membrane was eluted in 50 µl of RNase-free water, pre-heated to 60 ºC. The concentration and purity of the RNA was determined using the NanoDrop 1000 spectrophotometer (Thermo Scientific) that utilizes the full UV to visible light spectrum (220-750 nm) to analyze small sample volumes.

2.4.3 DNase treatment of RNA samples

qPCR is a highly sensitive method that can detect single molecules; therefore, it is essential to remove from our RNA samples any traces of genomic DNA that could act as template in the downstream applications. By treating 10 µg total RNA with 1 µl of the Turbo DNase from the Turbo DNA-free kit (Invitrogen), up to 2 µg of genomic DNA can be removed after incubating the 50 µl reaction at 37 ºC for 30 minutes. DNase is a recombinant versatile endonuclease with low specificity, which cleaves the phosphodiester bonds between nucleotides of double stranded DNA [29]. The amounts of reagents needed to digest each DNA are listed in the Table 4.

Table 4: Components for DNA digestion

Reagent	**Amount**
MilliQ	Adjust to final volume of 50 µl
10x Turbo DNase buffer	5 µl
Total RNA	10 µg
Turbo DNase	1 µl

The digestion is stopped by adding 5 µl of a special DNase inactivation resin that removes the DNase and divalent cations from the sample, eliminating the factors that could potentially catalyze RNA degradation over time. To concentrate the diluted DNase-treated RNA, the sample is precipitated by incubating for 1 hour at -80 °C in a solution with high salts, ethanol and glycogen. After centrifugation, the RNA pellet is washed with 70% ethanol, followed by resuspension of the final RNA pellet in 10 µl of MilliQ water warmed to 65 °C. Finally, the concentration and purity were determined on the NanoDrop 1000.

2.4.4 cDNA synthesis

Next, we followed the protocol from TaqMan Reverse Transcription Reagents (Applied Biosystems) to generate cDNA, the template for the following qPCR experiment. Depending on the concentration, each RNA sample was diluted appropriately to generate a working solution of 0.4 µg/µl. A total of 2 µg of each RNA sample was then aliquoted into duplicate 200 µl thin-wall PCR tubes. In order to minimize pipetting errors, a master mix (Table 5) was created with all of the components needed to complete the cDNA synthesis of the six RNA samples. To observe the effects of any contaminating genomic DNA in the RNA samples, the same master mix was prepared but with water replacing the reverse transcriptase (-RT). Finally, 15 µl of either the +RT or -RT master mix was added to the appropriate RNA samples, which were then incubated in a PCR machine set to the parameters outlined in Table 6.

Table 5: RT master mix

Component	1 rxn	[Final]	6+1 rxns
10X RT Buffer	2.0 µl	1x	14 µl
25 mM $MgCl_2$	1.4 µl	1.75 mM	9.8 µl
10 mM dNTP mix (2.5 mM each)	4.0 µl	0.5 mM each	28 µl
RNase Inhibitor (20 U/µl)	1.0 µl	1.0 U/µl	7 µl
MultiScribe™ RT (50 U/µl) *	1.0 µl	2.5 U/µl	7 µl
50 µM random hexamers	1.0 µl	2.5 µM	7 µl
MilliQ	fill up to 15 µl		

* - MultiScribe™ Reverse Transcriptase is a recombinant Murine Leukemia Virus reverse transcriptase (MuLV RT).

Table 6: RT incubation parameters

Temperature	Time
25 °C	10 minutes
37 °C	30 minutes
95 °C	5 minutes
4 °C	indefinitely

In relative qPCR we calculate how much the target expression changes during RNAi induction, compared to a robust internal gene expression that remains relatively constant under these deteriorating conditions (in our case – 18S rRNA and β-tubulin control housekeeping genes). For our experiment, cDNA samples (both +RT/-RT) used to amplify ATP11 or ATP12 needed to be diluted 1:10 with MilliQ water, while cDNA for internal references included 18S rRNA and B-tubulin was diluted 1:500. 2 µl of each appropriately diluted sample was pipetted in triplicate into a 96 well plate. The -RT RNA samples for each condition were only pipetted once. Then 18 µl of a master mix, prepared as indicated in the Table 7, was added to each well.

Table 7: SYBR Green I master mix

Reagent	Volume	12+1 rxns
2x SYBR Green I master	10 µl	130 µl
1.5 µM forward primer	4 µl	52 µl
1.5 µM reversed primer	4 µl	52 µl
Total	18 µl	234 µl

The plate then was sealed, centrifuged and placed in the Light Cycler 480 (Roche) for qPCR with the following parameters (Table 8):

Table 8: Roche Light Cycler 480 parameters

Step		Temperature	Time
Pre-incubation		95 °C	10 minutes
Amplification	**45 cycles**	95 °C	10 seconds
		60 °C	10 seconds
		72 °C	10 seconds

2.4.5 Calculating fold changes in target transcripts

From the qPCR amplification plots generated from the software on the Roche Light Cycler 480, we can now begin a series of calculations that will determine the fold change of our target transcripts relative to our internal control transcripts. These calculations are based on the Pfaffl method [30]. In real-time qPCR, the DNA sample is analyzed while the rection is in progress, by the growth of a signal from a fluorescent dye. Ideally, the fluorescence of each target should always be equal to 2, as if the amount of DNA would double after each of the cycles. However, in reality there is no such high accuracy for the primers to anneal, and the characteristics of DNA polymerase can slightly deviate. Therefore, it is always important to take into the account PCR efficiency value, while comparing the amount of DNA amplified using different sets of primers.

Another important task in our calculations was to determine the Cp value by using the default Light Cycler 480 software. This program randomly selects an arbitrary line that crosses all the PCR curves through the exponential phase, representing a constant fluorescence threshold value through all datasets. Then the software calculates the number of the cycle where the fluorescence crosses this threshold in each sample (Figure 10).

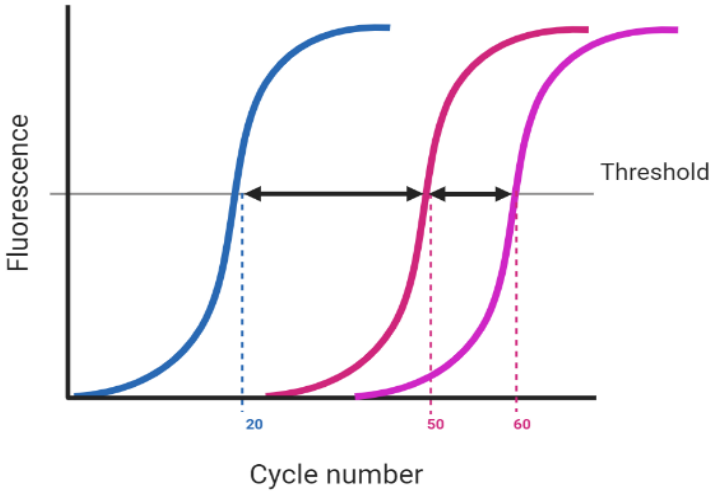

Figure 10: Processing of qPCR output (*generated using BioRender*).

Finally, the observed values were plugged into the formula below (Eq. 1). Here, the average Cp of each induced sample is subtracted from that of the non-induced cell lines for both the target and reference genes (ΔCp). The efficiency target is the PCR efficiency calculated for each distinct primer sets. These values depict how well the ATP11 and ATP12 transcript was depleted after two or four days of induced RNAi compared to the levels of transcript present in the noninduced RNAi samples.

$$Ratio\ treated/untreated = \left(\frac{Efficiency_{target}^{\Delta Cp\ target}}{Efficiency_{reference}^{\Delta Cp\ reference}} \right) \qquad (1)$$

2.5 Western Blot

Western blot is a widely used laboratory technique in which proteins can be separated based on their size and then detected by visualizing the target proteins with primary and secondary antibody on a solid support, usually polyvinylidene difluoride (PVDF) membrane. For this project, we wanted to observe if the targeted RNAi depletion of the F_1-ATP synthase assembly subunits ATP11 and ATP12 affected the expression of various protein constituents of the enzyme. $1x10^8$ cells from the ATP11 & ATP12 RNAi cell lines that were either noninduced or induced with tetracycline for 2, 4 or 6 days were harvested by centrifugation at 1300 xg for 10 minutes at 4 ºC. The media was then decanted and the remaining proteins from the media were washed away by resuspending the cell pellet in isotonic tris-buffered saline (PBS) and repeating the centrifugation step. After discarding the aqueous phase, the cell pellets were resuspended in PBS and a loading dye (Table 9) containing sodium dodecyl sulfate (SDS).

Table 9: 3x SDS-loading buffer composition

Reagent	**[Stock]**	**Amount**	**[Final]**
Tris (pH = 6.8)	1 M	7.5 ml	0.15 M
SDS	288.37 g/mol	3.0 g	6%
Glycerol	80%	18.75 ml	30%
DTT	154.25 g/mol	2.31 g	0.3 M
Bromophenol blue	2%	500 µl	0.02%
MilliQ H_2O	bring final volume to 50 ml		

SDS is a commonly used anionic detergent that is used to lyse intact cells and denature proteins by coating them in a negative charge. By applying a charge that propels the denatured proteins to move through a porous polyacrylamide gel, we are able to resolve the proteins based strictly on their size. To further denature proteins, dithiothreitol (DTT) in the loading dye reduces structural disulfide bonds. Glycerol helps the sample to sink into the well of the gel and bromophenol blue acts as a dye for the leading edge of the protein sample, as it migrates through the gel. Finally, the samples are incubated for 5-7 minutes in a heat block set at 97 °C to continue the denaturization process and diminish sample viscosity caused by the unwound genomic DNA.

The denatured protein samples from whole cell lysates were then resolved on pre-cast 4-20% gradient Tris-glycine polyacrylamide gels. The gels were submerged into a running buffer containing more SDS to ensure the proteins stay denatured as they navigate through the gel. After cleaning the wells by pipetting up and down to remove traces of acrylamide, $1x10^7$ cells were loaded on a gel alongside with 4 µl of the Prestained Protein Ladder (PageRuler). The gel was run under constant voltage (120 V) until the leading dye front of the samples began to exit the bottom of the gel.

Since the gel is very fragile, the proteins needed to be transferred to a sturdier membrane which is more suitable for downstream manipulations. For this, we were using a so-called wet transfer, in

which the gel and PVDF membrane are submerged into a transfer buffer surrounded by supporting materials that together create a plate-sandwich (Figure 11). The sandwich blots were inserted into a transfer apparatus filled with 1x transfer buffer through which 90 V were applied for 90 minutes. It was important to orient the sandwich correctly into the transfer apparatus so the negative charges emitting from the anode first passed through the gel, propelling the negatively charged proteins to transfer onto the membrane located on the cathode side of the gel. Also, the side of the membrane facing the gel was marked beforehand, so it was obvious which side contained the proteins to probed with antibodies upon completion of the transfer.

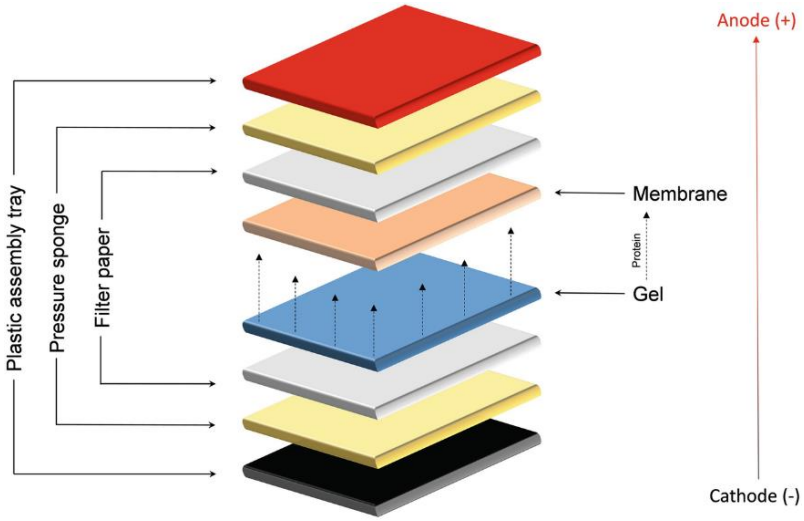

Figure 11: Western blot set-up (*Martins-Gomes C., Silva M.A., (2018) Western Blot Methodologies for Analysis of In Vitro Protein Expression Induced by Teratogenic Agents*).

After blotting, the device was disassembled and membranes were incubated with 45 ml of 5% skimmed milk on a rotating platform for 1 hour at room temperature. The abundant casein in milk saturates the free binding sites on the membrane, disabling the nonspecific attachment of primary and secondary antibodies and thus blocking unwanted background signal. The milk was then dissolved in a PBS-T – a mixture of phosphate-buffered saline, which provides isotonic solution and Polysorbate 20 (also known as Tween 20), that acts as a detergent, increasing the specificity of the antibodies by pulling over weak interactions from the blot (Table 10).

Table 10: PBS-T composition

Reagent	**[Stock]**	**Amount**	**[Final]**
NaCl	58.44 g/mol	8 g	137 mM
KCl	77.55 g/mol	0.2 g	2.7 mM
Na_2HPO_4	141.96 g/mol	1.44 g	10 mM
KH_2PO_4	136.086 g/mol	0.24 g	1.8 mM
Tween 20	1227.54 g/mol	1 ml	0.1 %
MilliQ H_2O	bring final volume to 1 L, adjust pH to 7.2		

Upon completion of the blocking, the milk was decanted and replaced with 5 ml of fresh milk, into which the primary antibodies were diluted. In the lab, we have generated rabbit polyclonal antibodies to the F_1-ATP synthase subunits β, p18 and both the N-terminal and C-terminal peptides of α. We also have antibodies raised against subunits of the peripheral stalk, namely OSCP and Tb2. Finally, a mouse monoclonal antibody that detects the abundant housekeeping protein mitochondrial heat shock protein, 70 kDa (mtHSP70) was used as a loading control. Based on prior experience with the avidity of these antibodies and the abundance of their protein targets, we used the following dilutions for each antibody: β (1:5000), p18 (1:2000), C-term α (1:100), N-term α (1:1000), OSCP (1:2000), Tb2 (1:2000) and mtHSP70 (1:5000).

The membranes were rotated for 1 hour at room temperature and then washed several times with 20-25 ml of PBS-T to remove unbound primary antibodies and thereby minimize background noise during the subsequent visualization. To amplify the signal of the primary antibody, we repeated the same procedure with secondary goat antibodies generated either against rabbit polyclonal or mouse monoclonal antibodies. Each of the secondary antibodies were diluted 1:2000 in 5 ml of 5% skimmed milk (Figure 12) and incubated with the blots at room temperature for 1 hour on a rotating platform. Importantly, these secondary antibodies were conjugated with horse radish peroxidase (HRP), an enzyme that oxidizes the substrate luminol to generate light emitted at 428 nm. This light signal can then be captured on X-ray film or by a digital imager. After 1 hour incubation, excess antibodies were washed off the membrane with PBS-T. Then the chemiluminescence enhancer (Clarity ECL from BioRad) containing the luminol substrate was applied to the blot. The signal was then visualized using the Chemidoc MP system from BioRad.

The resulting images were then normalized and quantified by ImageLab software (BioRad). For longer storage of the blots, they were washed with PBS-T and then submerged in the same buffer and placed at 4 °C.

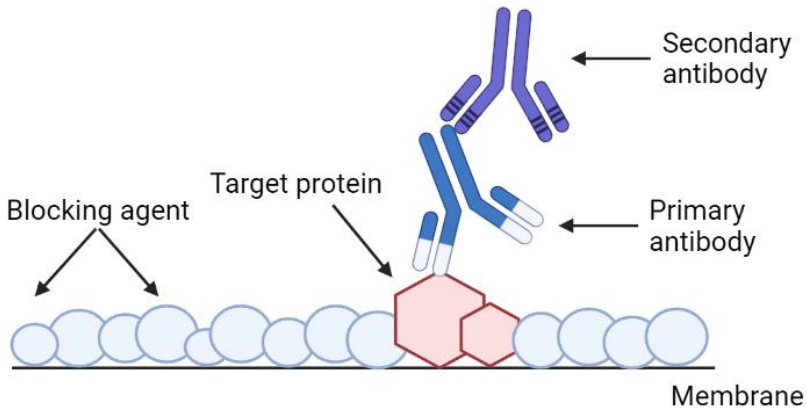

Figure 12: Western blot schematic (*generated using BioRender*)

2.6 Blue Native Polyacrylamide Gel Electrophoresis

While SDS-PAGE will allow us to examine the steady-state levels of individual ATP synthase subunits, we are more interested in what the depletion of specific F_1 assembly factors does to the stability of the enzyme as a whole. In other words, we want to examine the integrity of a large native protein complex and determine if the loss of ATP11 or ATP12 results in any subcomplexes that could reveal information about the mechanism of ATP synthase assembly. For this, we performed Blue Native Polyacrylamide Gel Electrophoresis **(**BN-PAGE), the laboratory technique which allows for the characterization of the integrity of large native protein complexes in their enzymatically active state. BN-PAGE does not require any ionic detergents such as SDS, but rather special Coomassie Blue-G250 dye, which coats the protein complexes with necessary negative charge for the migration in the gel. The Coomassie dye binds to proteins through Van der Waals forces and ionic interactions that occur between the sulfonic acid groups of the dye and the positive amine groups of the protein (Figure 13). In BN-PAGE, the protein complexes tend to migrate according to the pore size of the gradient gel until they reach the pore size limit point. This provides the high-resolution separation of native protein complexes based on their molecular weight.

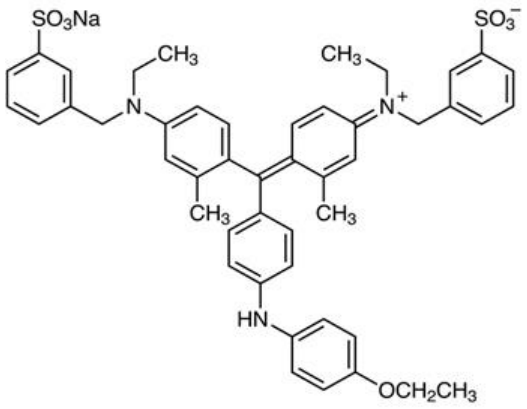

Figure 13: Coomassie Blue-G250 dye chemical structure (*TCI chemicals*)

2.6.1 Mitochondria Isolation

Since we are interested in the native state of a mitochondrial protein complex, we first isolated mitochondria from *T. brucei* parasites to enrich our protein samples for ATP synthase. This crude mitochondrial prep was performed under hypotonic conditions that causes water to rush into the parasite and swell the plasma membrane. This cell membrane is then ruptured when the bloated cells are placed under high pressure as they are passed through a 25G needle. The solution is then returned to isotonic conditions to prevent the lysis of any organelles, which are isolated from the cytoplasmic material by a differential centrifugation step. The chemical composition of the buffers required for this method are listed below (Table 11).

Table 11: Working solutions for mitochondria isolation

Name of a stock	Component	[Final]
NET	NaCl	0.15 M
	EDTA	0.1 M
	Tris-HCl, pH 8.0	10 mM
DTE	Tris-HCl, pH 8.0	1 mM
	EDTA	1 mM
STM	Sucrose	250 mM
	Tris, pH 8.0	20 mM
	$MgCl_2$	2 mM
STE	Sucrose	250 Mm
	Tris, pH 8.0	20 mM
	EDTA	10 mM

Since the density of cells per volume of buffer are essential to generate the correct force to lyse the parasites, we harvested $2.5x10^8$ cells that were either noninduced or RNAi induced with tetracycline for 1, 2 or 4 days. After a 1300 xg centrifugation for 10 min at 4 ºC, the cell pellets were resuspended in ice-cold NET solution and spun again under the same parameters. EDTA in this solution chelates divalent cations, which reduces the solutes in the buffer, making it hypotonic compared to the parasites.

After resuspending the cell pellets in the hypotonic DTE buffer, the *T. brucei* cell membrane was disrupted by passing the bloated cells through a 25G needle 3 times. In order to prevent further swelling and mitochondrial lysis, 1.5 ml of the lysate was immediately mixed with 180 µl of 60% sucrose to return the solution to isotonic conditions. To enrich for mitochondria by removing the cytosolic material, a high-speed centrifugation step was performed to pellet the organelles in the sample. After spinning for 15,000 xg for 10 min at 4 ºC, the soluble cytosolic fraction was decanted, while the organellar pellet was resuspended in the isotonic STM buffer. The release of unwound genomic DNA after cell lysis makes the solution very viscous. Since this can act like a net and pull down other contaminants in the solution, we treated the lysate with DNase. Because DNase activity relies on cations, the organellar pellet was resuspended in the isotonic STM buffer containing $MgCl_2$. Additionally, 1.5 µl of 1M $MgCl_2$, 1.5 µl of 0.1 M CaCl and 0.7 µl DNase (10 mg/ml) were added and the sample was incubated for 1 hour on ice.

The DNase treatment was terminated by adding and equal volume of STE, which contains the Mg chelator EDTA. The organellar pellet was then washed repeatedly in the isotonic STE buffer (15,000 xg for 10 min at 4 ºC) until the pellet became firm. After the last spin, the STE was decanted and the organellar pellet was frozen in liquid nitrogen and then stored at -80 °C.

2.6.2 Organellar lysis and protein concentration measurements

Since ATP synthase is a membrane embedded protein complex, we need to lyse the organellar pellet and then solubilize the membrane proteins. This was performed by resuspending the organellar pellet in 40 µl of 1M aminocaproic acid (ACA) and 10 µl of 10% dodecylmaltoside (DDM), added to its final concentration of 2%. While the detergent DDM lyses the mitochondrial membranes, the ACA acts as a serine protease inhibitor and helps to solubilize membrane proteins. After a 1 hour incubation on ice, the sample was centrifuged at 12,00 rpm for 30 minutes at 4 ºC. The aqueous phase containing the solubilized proteins was then transferred to a new tube.

In order to compare how the integrity of the F_oF_1-ATP synthase changes as the assembly factors are depleted by RNAi, we need to ensure that equal amounts of material are loaded onto the gel for each sample. Since there are very few options available to control for equal loading between BN samples, it is critical to determine the protein concentration of each sample. Assuming the protein complexity remains generally constant between the RNAi time points, we can then load consistent amounts of total solubilized organellar proteins. For this purpose, we followed the protocol outlined for the Pierce BCA protein assay kit. This method is based on the well-known biuret reaction where the peptide bonds in proteins reduce Cu^{+2} to Cu^{+1} under alkaline conditions [31]. One cuprous ion causes the chelation of two molecules of BCA and the reaction product of this assay becomes purple-colored. This water-soluble complex exhibits a strong absorbance at 562 nm and the assay is nearly linear with increasing protein concentrations over a broad working range (20-2000 µg/mL) [32]. Samples with unknown protein concentrations are calculated based on the standard curve of a common protein, such as bovine serum albumin (BSA). Therefore, a series of dilutions resulting in known BSA concentrations are prepared in 1M ACA and then assayed alongside our protein samples (Table 12).

Table 12: BSA standards for BCA assay

Standard	[Final]	BSA*	1M ACA	Total volume
A	2000 µg/ml	10 µl 10% BSA	490 µl	500 µl
B	1500 µg/ml	7.5 µl 10% BSA	492.5 µl	500 µl
C	1000 µg/ml	5.0 µl 10% BSA	495 µl	500 µl
D	750 µg/ml	250 µl of B	250 µl	500 µl
E	500 µg/ml	250 µl of C	250 µl	500 µl
F	250 µg/ml	250 µl of E	250 µl	500 µl
G	125 µg/ml	250 µl of F	250 µl	500 µl
H	25 µg/ml	50 µl of G	200 µl	250 µl
I (blank)	0 µg/ml	0 µl	200 µl	200 µl

* – 10% BSA = 100 µg/µl

Then we mixed the two solutions provided by the kit to prepare the working reagent, which contained sodium carbonate, sodium bicarbonate, bicinchoninic acid and sodium tartrate in 0.1M sodium hydroxide with 4% cupric sulfate. While the BCA assay is linear over a wide range, we still need to estimate how much to dilute our protein rich samples to fall within this range. therefore, we chose to dilute the organellar samples 1:10 and 1:20 with 1M ACA. Following the microplate procedure outlined by the manufacturer, we pipetted equal volumes of each protein sample, as well as the BSA standards, into a 96 well microplate. Then, 200 µl of the working reagent was added to each well and mixed thoroughly. The plate was then covered with aluminum foil and incubated at 37 °C for 30 minutes. After cooling the plate to room temperature, the absorbance of each well was measured at 562 nm on a Tecan Spark plate reader. The absorbance values of the BSA standards were then plotted to generate a trendline through this calibration curve. The resulting slope-intercept equation was used in coordination with the absorbance values of the protein samples to calculate the final protein concentrations.

2.6.3 Electrophoresis, western blot and protein ladder visualization

Once the electrophoresis apparatus for the BN-PAGE was assembled, the upper buffer chamber was filled with the cathode buffer (50 mM Tricine, 15 mM Bis-Tris, 0.002% CBB G-250, pH 7.0), while the lower buffer chamber was filled with the anode buffer (50 mM Bis-Tris, pH 7.0). For the best resolution and detection of various subunits from the ATP synthase, it was previously determined that 4 µg of total protein from each sample should be loaded onto a pre-cast 3-12% Bis-Tris gradient Native PAGE Novex gel from Invitrogen. The calculated volume of these protein samples was mixed with 1.5 µl of a loading dye (0.5M ACA, 5% CBB G-250) and the remaining volume of the 20 µl sample was filled with 1M ACA. After incubating on ice for 10 minutes, the samples were loaded onto the gel alongside 10 µl of the Native Mark Unstained Protein Standard (Invitrogen). The gel was then run at a constant 150 V for 2.5 hours at 4 °C. Upon completion, the protein ladder was carefully excised from the rest of the gel so that it could be independently treated with Coomassie dye to visualize the bands. This procedure required rinsing the gel slice with dH_2O before incubating them with a fixing solution (Table 13) on an orbital shaker for 30 minutes.

Table 13: Fixing solution

Reagent	Volume	[Final]
dH2O	200 ml	
Methanol	250 ml	50%
Acetic acid	50 ml	10%

Next, the gels were immersed in a Coomassie dye solution (Table 14) and shaken for another 20-30 minutes.

Table 14: Coomassie dye solution

Reagent	Volume	[Final]
MilliQ	200 ml	
Methanol	250 ml	50%
Acetic acid	50 ml	10%
Coomassie G-250*	50 ml	10%

* - Coomassie dye was firstly dissolved in methanol, as it is not very soluble in H_2O.

After thoroughly rinsing off the Coomassie stain with water, the gels were left on the shaker overnight in a destain solution (Table 15). Finally, the Coomassie stained gels were visualized on the BioRad Chemidoc the next day.

Table 15: Destain solution

Reagent	Volume	[Final]
dH2O	880 ml	
Methanol	50 ml	5%
Acetic acid	70 ml	70%

Meanwhile, the remaining portion of the gels containing our resolved protein complexes were transferred to a PVDF membrane by the same principal described in §**3.5**, but this time at 4 °C. The membrane was then probed with the p18 and β antibodies at the dilution of 1:1000 and visualized on the Chemidoc (BioRad). As an additional loading control, an aliquot of the remaining protein samples prepared for the BN western blot analysis were mixed with the SDS-PAGE loading buffer and incubated for 9 minutes at 96 °C to denature the proteins. These samples were then resolved on a denaturing gel and probed with a suite of ATP synthase antibodies as described previously in §**3.5**.

2.7 Molecular cloning

My project began with the already genetically modified *T. brucei* cell lines that knockdown ATP11 and ATP12 by RNAi. As it will become evident in the Results section, we decided to target an alternative region of the ATP11 transcript by RNAi to deplete the gene product more efficiently. This section will highlight the methods I employed to generate this new ATP11 RNAi plasmid.

RNAi is a powerful molecular biology tool to rapidly discern the function of a protein. Fortunately, this defense pathway is intact in the early diverging *T. brucei*. Therefore, the regulatable expression of long double-stranded RNA (dsRNA) molecules targeting a specific mRNA can be transcribed from an RNAi plasmid integrated into the genome of the parasite. Believing these molecules to be viral in origin, the *T. brucei* RNAi defense mechanism employs dicer-like proteins to cleave the dsRNA into small interfering RNAs (siRNAs). These siRNAs are then loaded onto the RNA-induced silencing complex (RISC), where they duplex with the complementary mRNA. One component of RISC is the endonuclease Argonaut that cleaves the targeted transcript and thereby depletes the gene product.

2.7.1 RNAi plasmid construction

While there are several different types of plasmids capable of producing dsRNA in *T. brucei*, we utilize a plasmid termed pAZ055 (Figure 14), which was slightly modified in the Zíková lab from the Horn lab vector pRPa^{iSL} [34]. Transcription of this plasmid generates dsRNA in the form of a stem-loop within a single molecule. This is achieved by flanking a β-galactosidase (LacZ) fragment with two copies of the targeted gene sequence in reverse orientation to each other. Therefore, the annealing of the complementary target sequences at the ends of the RNA are connected via an internal loop containing the LacZ fragment. Transcription of the plasmid to produce the stem-loop RNA is initiated by an upstream rRNA promoter sequence previously characterized in *T. brucei*. In case the targeted gene product is essential to the parasite, this transcription needs to be tightly regulated. Thus, a tetracycline operator has been inserted immediately downstream of the rRNA promoter. Since the parental *T. brucei* cell line transfected with the pAZ055 plasmid already constitutively expresses the tetracycline repressor from bacteria, transcription is physically blocked when this protein binds the tetracycline operator sequence. Transcription can elegantly be initiated by adding tetracycline to the media. Upon entering the parasite, the antibiotic binds to the tetracycline repressor protein and causes a conformational change that releases the protein from the tetracycline operator. This leaves the *T. brucei* RNA polymerase unhindered to continue transcription of the RNAi molecule.

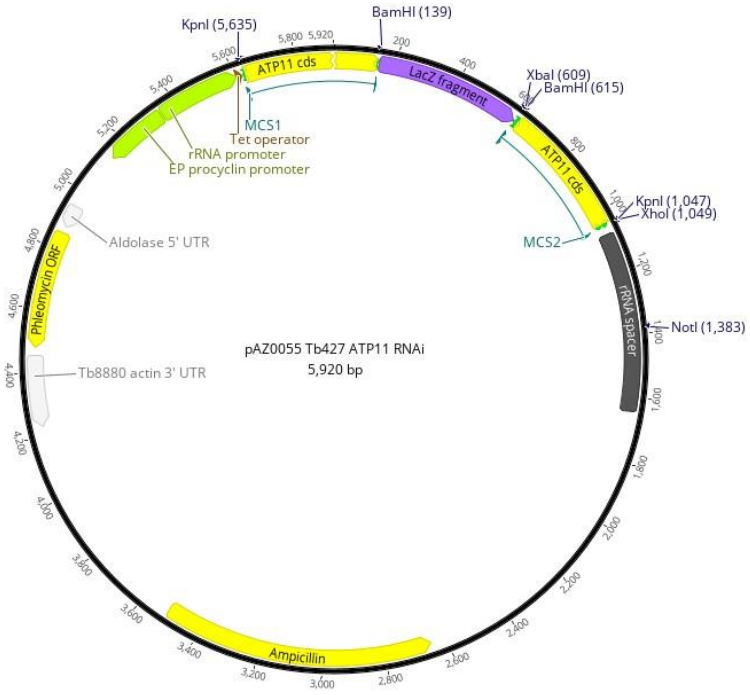

Figure 14: pAZ0055 ATP11 RNAi stem loop vector. The coding sequences for proteins are indicated with yellow block arrows, with the LacZ peptide highlighted in purple. The promoters are depicted with green block arrows, while the *T. brucei* untranslated regions are outlined in white block arrows. The rRNA spacer region is drawn with a grey box. The location of unique restriction sites are indicated by the name of the enzyme and the position within the plasmid sequence (*generated using Geneious*).

Other unique features of the pAZ055 RNAi plasmid include positive selectable markers for both bacteria and *T. brucei*. The plasmid encodes a secreted β-lactamase that degrades the antibiotic ampicillin, allowing only bacteria that retain the plasmid to grow. *T. brucei* can be selected by adding phleomycin to the media since the plasmid generates a protein that inhibits the antibiotic from inducing double-strand breaks in the genomic DNA. Since this gene product is expressed in *T. brucei*, it contains an upstream promoter for the abundant surface protein, EP procyclin, which is named for having numerous repeats of glutamate (E) and proline (P) amino acids. Furthermore, to increase the transcript stability of the selectable marker, the *T. brucei* aldolase 5' untranslated region and the actin 3' untranslated region flank the coding sequence. Finally, to generate stable cell lines for multiple downstream biochemical analyses, it is essential to integrate the pAZ055 RNAi plasmid into the *T. brucei* genome. Therefore, prior to *T. brucei* transfection, the vector is linearized with the FastDigest NotI restriction enzyme (Thermo Scientific), which recognizes a single restriction site (5'- GC/GGCCGC -3') located in the middle of a *T. brucei* rRNA spacer locus. This results in both ends of the linearized plasmid containing complementary sequences to the parasite genome, which allows for homologous recombination at the rRNA spacer locus.

2.7.2 Preparing the destination vector

The first process of the multistep cloning procedure was to prepare the pAZ055 RNAi plasmid. A -80 °C glycerol stock of *E. coli* containing the pAZ055 plasmid was streaked out on a semi-solid lysogeny broth (LB) agar plate (Table 16).

Table 16: Lysogeny broth media composition (pH = 7.3)

Reagent	**Amount**	**[Final]**
Tryptone	5 g	1%
Yeast extract	2.5 g	0.5%
NaCl	0.25 g	8.5 mM
Agar	7.5 g	
MilliQ H_2O	Fill up to 500 ml	

The selectable antibiotic ampicillin was embedded in the agar at a concentration of 100 µg/ml. The bacteria were incubated for ~16 hours overnight in the 37 °C incubator. We were careful not to allow the bacteria to overgrow, as the secreted β-lactamase would begin to accumulate around colonies containing the plasmid, creating a zone without the antibiotic that would allow for the growth of smaller satellite colonies that do not contain the plasmid. In order to preserve isolated colonies, the plates were incubated upside-down to avoid water condensation on the surface of the agar plate. To retain the viability of the bacterial colonies for up to six weeks, the agar plates were stored at 4 °C.

Next, we needed to isolate the plasmid DNA from the bacteria. To ensure we had enough plasmid for downstream manipulations, a single bacterial colony was picked with a pipet tip from the agar plate and transferred into an Erlenmeyer flask containing 50 ml of LB media containing 100 µg/ml ampicillin. The bacteria culture was then incubated for ~16 hours in a 37 °C shaking incubator. Plasmid isolation was then performed according to the instruction [35] manual provided with the GenElute HP Plasmid Midiprep Kit (Sigma). The cells were harvested by spinning the cells at 5,000 xg for 10 minutes at room temperature. After decanting the media, the cell pellet was resuspended in a solution containing Tris, EDTA, glucose and RNase A. The presence of RNase, an endonuclease that hydrolyzes the phosphodiester linkage at the 3´ end of pyrimidine nucleotides, eliminates all contaminating cellular RNA once the cells are lysed. Cell lysis occurs when they are incubated for 4 minutes at room temperature with a solution containing NaOH and SDS. The SDS solubilizes the membrane and denatures most of the proteins from the cells, which helps eliminate the proteins from the plasmid later in the process. NaOH helps to break down the cell wall, but more importantly, it disrupts the hydrogen bonding between the DNA bases, converting the dsDNA to ssDNA. The immediate addition of potassium acetate in the next step decreases the alkalinity of the mixture, thereby allowing ssDNA to re-anneal. However, while it is relatively easy to reconstitute the short circular plasmid DNA strands, it is almost impossible to properly anneal huge genomic DNA stretches. This ensures that the double-stranded plasmid remains soluble, while the genomic DNA, lipids and other denatured proteins stick together and form a white precipitant due to hydrophobic interactions. After the addition of a binding solution, the mixture was transferred to a syringe where the precipitated agglomerate floated to the top. The aqueous phase containing the soluble plasmid was then filtered and placed onto a spin column containing a silica resin that selectively binds the plasmid DNA. The spin column was washed twice with an ethanol solution before transferring the spin column to a new collection tube to remove any traces of ethanol. The plasmid DNA was finally eluted from the column with a pre-warmed elution solution. The purity and concentration of the plasmid DNA was analyzed on the NanoDrop.

The generation of an ATP11 pAZ055 stem-loop RNAi vector requires two sequential cloning steps that insert the same RNAi targeting sequence in opposite orientations. To achieve this, we decided to utilize two multiple cloning sites (MCS) flanking the lacZ fragment, specifically the unique BamHI and Kpnl restriction sites within the upstream MCS1 and the Xbal and Xhol sites in the downstream MCS2. To prepare for the insertion of the forward ATP11 targeting sequence in MCS1, the isolated pAZ055 plasmid was digested with the BamHI and Kpnl enzymes in a reaction outlined in Table 17. The components were mixed gently, briefly centrifuged and incubated at 37 °C in a heat block for 1.5 hour.

Table 17: Components for Fast DNA digestion

Reagent	Volume/Concentration
10x Fast Digest Green Buffer	5 µl
Restriction enzymes	4 µl (2 µl each)
Plasmid DNA	10 µg
Nuclease-free water	up to 50 µl

Despite optimal conditions, the digest will be less than 100% effective. For this reason, we need to resolve the DNA molecules on an agarose gel to isolate the properly digested pAZ055 backbone. Therefore, digested pAZ055 was loaded on an 0.8% agarose gel, which was prepared from 0.56 g of agarose boiled in 70 ml Tris-acetate-EDTA (TAE) buffer (Table 18). To dissolve the agarose in TAE, it was heated in a microwave until it just began to boil. Then it was allowed to cool before adding the heat labile ethidium bromide. Due to its ring structure resembling a nucleotide base, this fluorescent dye intercalates with double stranded DNA. Therefore, after resolving the DNA for 1.5 hours at 90 V on the agarose gel, the DNA fragments could be visualized on the Chemidoc using a UV light source.

Table 18: TAE buffer composition

Reagent	[Stock]	Amount	[Final]
Tris	121.14 g/mol	4.84 g	40 mM
Glacial acetic acid	60.05 g/mol	1.142 ml	20 mM
EDTA	0.5 M	2 ml	1 mM
MilliQ H_2O		Fill up to 1 L	

To determine the sizes of the DNA fragments, 10 µl of the GeneRuler 1 kb Plus DNA Ladder (Thermo Scientific) was also included. Finally, as a control, uncut pAZ055 plasmid was also resolved on the gel. A photographic document of the final gel was captured using the Chemidoc MP Imaging System. Then the gel was placed on an open UV light box that illuminated the DNA molecules. Bands of the expected size were removed with a clean razor blade and placed in a 2 ml test-tube.

To extract the desired DNA from the agarose, we followed the instruction manual provided with the GenElute Gel Extraction Kit (Sigma). After weighing the gel slice, 3 gel volumes of the Gel Solubilization Solution were added and the mixture was incubated at 60 °C for 10 minutes. When the gel slice was completely dissolved, it was briefly vortexed and cooled. The solution was inspected to ensure that it remained a yellow color, indicating that the pH range was between 4-5, which is optimal for DNA binding. One gel volume of 100% isopropanol was then added to the solution and mixed until homogenous. The solubilized digested DNA was then added to a pre-equilibrated spin column, washed with Washing Solution and centrifuged at 15.000 xg for 1 minute at 4 ºC. To minimize the risk of any ethanol contamination, the spin column was moved to a fresh collection tube. Then 50 µl

of the Elution Solution was added to the center of the membrane and allowed to incubate for 1 minute. For the better DNA recovery, an aliquot of the Elution Solution was pre-heated to 65 °C. Finally, the purity and concentration of the plasmid DNA was determined on the NanoDrop.

2.7.3 Primer design

The length of the dsRNA should be between 400-600 base pairs (bp) for the optimal RNAi depletion of a target gene in *T. brucei*. It has also been demonstrated that targeting various regions of the coding sequence can lead to different levels of RNAi depletion for the same gene product. Therefore, in order to increase the RNAi efficiency, we designed new primers to target a different region of the ATP11 coding sequence (Figure 15).

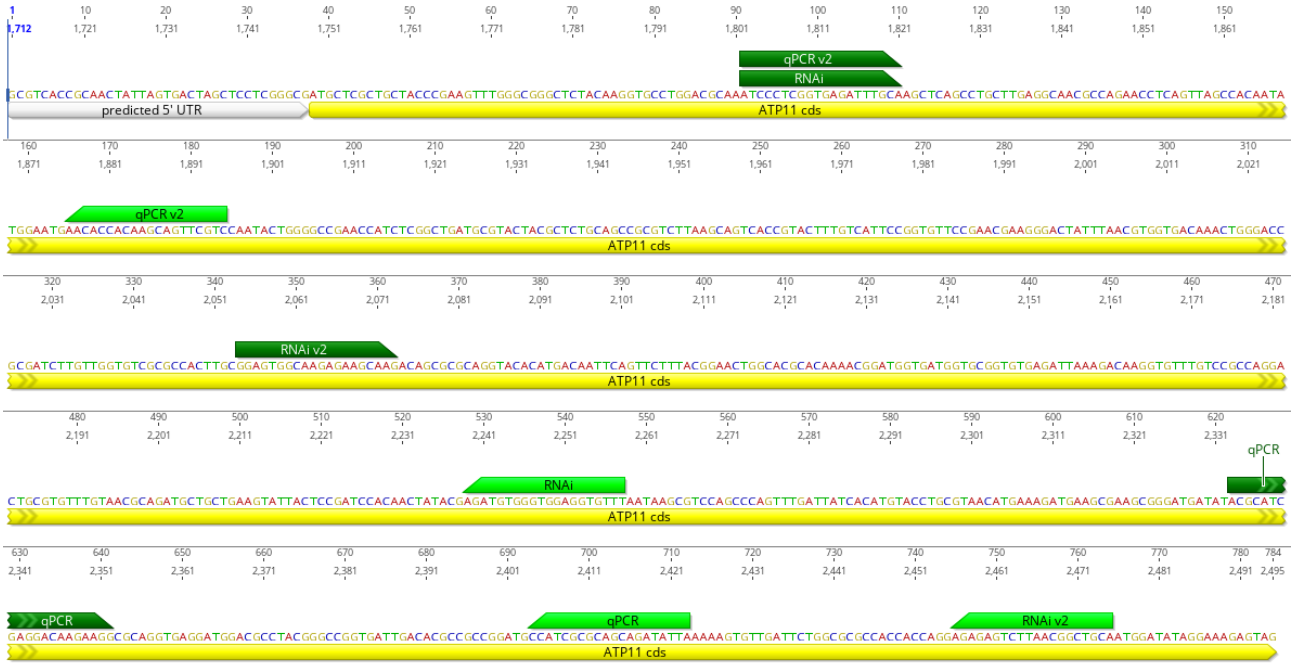

Figure 15: *T. brucei* ATP11 coding sequence. Yellow arrow represents the coding sequence, dark and light green arrows stand for the forward and reverse primers (v2 – newly designed), respectively (*generated using Geneious*).

Since we do not have antibodies to the ATP11 protein, we will also need to design primers that will be used in qPCR to quantify the level of transcript depletion. This amplicon should be between 80-120 bp and amplify a region of the coding sequence other than the portion targeted for RNAi, which will be synthesized in large amounts and will mask the true quantity of the endogenous transcript.

With these restrictions in mind, we utilized the powerful Primer3 software to first suggest the best primer pairs to amplify a region of ATP11 to target by RNAi. Some basic features of optimal primers include the following: complementary annealing length of ~20 bp, G/C content of ~50%, minimal predicted hairpins within the primer and a 3' G/C terminal nucleotide to increase the stability of the duplexed primer/template immediately before DNA polymerase extension. Therefore, we selected the new primers pair AZ1148 (forward) and AZ1149 (reverse), which would amplify 422 bp of the

5’ end of the ATP11 coding sequence. This left enough real estate to design our qPCR primers (AZ1150 and AZ1151) to amplify 94 bp of the 3’ end of the coding sequence. Next, we needed to include the proper restriction sites at the 5’ ends of the RNAi primers. These sites are dictated by the sites available within MCS1 and MCS2. Further, the selected restriction sites cannot be contained within the RNAi amplicon. To minimize the PCR optimization, we designed the PCR primers so the resulting amplicon could be inserted in either the forward direction (MSC1) or the reverse direction (MCS2). Finally, the pair of restriction sites used to insert the RNAi amplicon into each cloning site should be unique to ensure proper directional cloning. For cloning into MCS1, we chose KpnI for the 5’ end and BamHI for the 3’ end. After inserting the RNAi amplicon into MCS1 using these enzymes, we needed to use alternative sites for cloning into MCS2. Therefore, we chose 5’ XhoI and 3’ XbaI. Finally, we also needed to include 4 additional nucleotides on the 5’ end of each primer to generate a long enough sequence for the restriction enzyme to bind tightly. Since these 4 nucleotides are not sequence specific, they can be selected in a way that helps rebalance the GC content of the entire primer to match that of the other primer pair. Our primer design results in two 36 bp primers with ~55% G/C content (Figure 16).

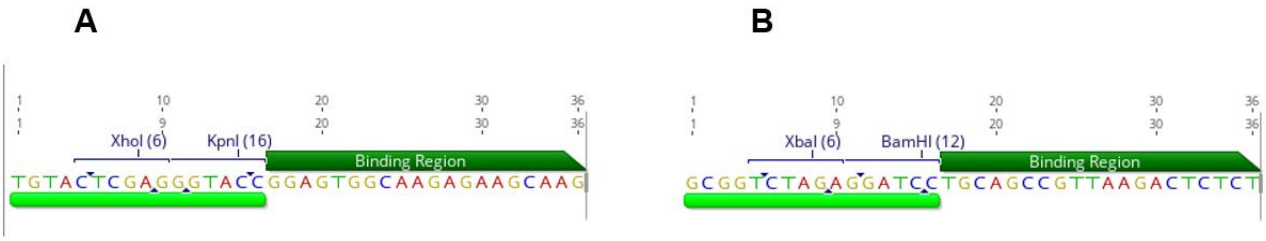

Figure 16: Designed RNAi primers pair. A) Forward AZ1148 and B) reverse AZ1149 36 bp primers. Prior to the binding region (dark-green) corresponding restriction sites are shown, together with four extra nucleotides (*generated using Geneious*).

2.7.4 Preparing the amplicons

Using the RNAi primers outlined above, we could perform PCR to amplify the ATP11 specific sequence from isolated *T. brucei* genomic DNA (gDNA). Since the method of RNAi can still function efficiently even if there is an occasional error produced by the DNA polymerase, we decided to use the economical and robust One *Taq* DNA-polymerase (NEB). According to the manufacturer’s instructions, the following amounts of each PCR reagent (Table 19) were mixed into sterile, thin-walled PCR tubes. These reaction tubes were then placed into a T1000 thermo cycler (BioRad) that was already programmed with the cycling parameters (Table 20) outlined for our DNA polymerase and the predicted length of the amplicon.

Table 19: PCR reaction setup

Component	Volume	[Final]
5x One *Taq* Standard reaction buffer	10 µl	1x
10 mM dNTPs	1 µl	200 µM
10 µM Forward primer	1 µl	0.2 µM
10 µM Reverse primer	1 µl	0.2 µM
One *Taq* DNA Polymerase	0.25 µl	1.25 units/50 µl PCR
***T. brucei* gDNA template (50 ng/µl)**	2 µl	100 ng
Nuclease-free water	up to 50 µl	

Table 20: PCR parameters

Step	Temperature	Time
Initialization	94 °C	30 seconds
30 cycles - **Denaturation** - **Annealing** - **Extension**	 94 °C 52 °C 68 °C	 15 seconds 30 seconds 40 seconds
Final extension	68 °C	5 minutes
Hold	4-10 °C	

To visualize the amount and quality of the PCR amplification, we resolved the amplicon on a 1% agarose gel that was prepared with the components listed in Table 21. After resolving the DNA obtained from the whole PCR reaction for 1 hour at 90 V on the agarose gel, the DNA fragments were visualized on the Chemidoc using a UV light source. To verify the correct size of the detected amplicons, 10 µl of the GeneRuler 1 kb Plus DNA Ladder was also run alongside the PCR products.

Table 21: Recipe for 1% agarose gel

Reagent	Volume	[Final]
TAE buffer	70 ml	
Agarose	7 g	1%
Ethidium bromide	1 µl	

If the PCR reactions successfully produced a predominant band of DNA at the expected size, the amplicon needs to be extracted from the agarose using the GenElute Gel Extraction Kit (Sigma) as described previously in §**3.7.2**. The isolated DNA is now easily manipulated with restriction enzymes to create sticky single-stranded overhangs that can be used to ligate the DNA fragments into the prepared pAZ055 plasmid. The restriction digests were performed as outlined previously in §**3.7.2**, but this time the digested DNA was isolated using the GenElute PCR Clean-up kit (Sigma). This is another spin column system that works on a similar principle as the previous kits, but this time it removes the enzymes and short digested DNA ends. First, the membrane in the spin column was activated by washing with a column preparation solution. Then, 5 volumes of the Binding Solution

were added to the entire volume of the gel extracted PCR amplicon before it was transferred to the spin column and bound to the silica membrane of the column. The membrane was washed with the Washing Solution, transferred to the new collection tube and eluted with the 50 µl of pre-warmed Elution Solution. The purity and concentration of the genomic DNA was again determined on the NanoDrop.

2.7.5 Ligation and transformation

After both the destination vector pAZ055 and the ATP11 RNAi insert were digested and purified, the complementary single-stranded overhangs at the ends of each DNA fragment were annealed and then ligated with the T4 DNA ligase (Promega). This enzyme creates a phosphodiester bond between the 5 -phosphate and the 3 -hydroxyl groups of adjacent nucleotides, thus covalently joining two DNA molecules. According to the manufacturer's instructions, the ligase is most efficient when the reaction contains a 3:1 molarity ratio between the insert and vector [36] and the total amount of DNA is ~100 ng. To calculate the molarity of a DNA fragment, the following equation (Eq. 2) was applied:

$$\text{Molar mass (nM)} = \frac{\text{DNA concentration ng/ul} * 1000}{0.325\ \text{g/mol} * \#\text{base pairs}} \qquad (2)$$

Since the total ligation reaction is only 10 µl, there is only 8 µl remaining for the digested insert and vector after including 1 µl of the ligase and 1 µl of the 10x buffer. If the yield from the purified vector was quite reasonable, we first calculated the amount of insert needed if the reaction contained just 1 µl of the vector. If this total volume was under 8 µl, then the remaining volume was provided by nuclease-free water. After mixing each of the ligation components, the samples were incubated overnight at 4 °C. An additional ligation was created with the same components, except the ATP11 RNAi insert was omitted. This served as a negative control and demonstrated how much undigested plasmid contaminated our sample.

To amplify the number of correctly ligated ATP11 RNAi plasmids, we need to coerce bacteria to uptake foreign DNA and create numerous copies that can later be extracted. This transformation process is enhanced by using chemically competent XL-1 blue *E. coli* that were previously treated with calcium chloride to facilitate DNA binding to the cell surface. After the 50 µl aliquots of the cells were thawed on ice, they were gently mixed with 3 µl of the ligation reaction and incubated on ice for another 20 minutes. Bacteria coated in DNA were then heat shocked in a 42 °C water bath for 45 seconds and then immediately placed on ice for 2 minutes. Such an abrupt change of temperature created a pressure difference between the inside and outside of the cells, which in turn caused the formation of pores in the cell membrane through which supercoiled plasmid DNA could enter. After the recovery period on ice, the bacteria were grown in a 37 °C shaking incubator for 45 minutes with

250 µl of the nutrient-rich Super Optimal broth with catabolite repression (SOC). Then 250 µl of the transformed cultures were spread onto an agar plate containing the selectable antibiotic ampicillin. The bacterial plates were incubated upside-down in the 37 °C incubator for 16 hours before being placed at 4 °C for long-term storage.

2.7.6 Isolated plasmid preparation from selected bacterial colonies

In order to determine if any of the individual bacterial colonies on the transformation plates contained the pAZ055 plasmid with ATP11 RNAi inserted into MCS1, we digested isolated plasmids and screened for the correct DNA fragments. Using a pipet tip, several individual colonies were picked from the transformation plates, streaked onto a new agar plate as a replicate and then seeded into a 5 ml overnight bacterial culture consisting of LB supplemented with ampicillin. Plasmid isolation was then performed with the GenElute HP Plasmid Miniprep Kit (Sigma). The protocol was based on the previously used silica-binding technology and the convenience of a spin column format. Briefly, the *E. coli* culture was harvested by centrifugation and subjected to a modified alkaline-SDS lysis procedure. This was followed by the adsorption of the plasmid DNA onto the silica membrane in the presence of high salts. Contaminants were then removed by a spin wash step. Finally, the bound plasmid DNA was eluted with 100 µl of an elution buffer containing a 10 mM Tris-HCl solution, pH 8.5 [35]. The concentration and purity of each sample was measured on the NanoDrop. 1 µg of plasmid DNA was then digested with the same restriction enzymes used for cloning (BamHI and Kpnl) into MCS1. DNA fragments were then resolved on a 1% agarose gel and visualized on the Chemidoc. One of the clones containing DNA fragments of the expected sizes was then chosen for subsequent cloning steps.

To complete the cloning of the stem-loop ATP11 RNAi vector, the same steps outlined above were repeated using the restriction enzymes XbaI and XhoI. Both the ATP11 amplicon and the newly generated pAZ055 ATP11 MCS1 plasmid were digested and ligated to insert the second ATP11 RNAi fragment in the reverse orientation at MCS2. The ligated DNA molecules were transformed into bacteria and the resulting colonies were screened for the correct RNAi plasmids by restriction digest. A positive plasmid clone was then selected for sequencing to confirm the proper integration of both ATP11 RNAi inserts in the pAZ055 plasmid.

2.7.7 Plasmid sequencing

To further validate that both ATP11 RNAi fragments were integrated into the pAZ055 plasmid in reverse orientation with minimal discrepancies in the predicted sequences, we submitted our samples for sequencing to SeqMe s.r.o. (Dobris, Czech Republic). Since the region we would like to sequence will make a double-stranded DNA hairpin structure that will interfere with the processivity

of the DNA polymerase used during sequencing, we employed SeqMe's HairpinSeq protocol. This method utilizes the addition of a variety of chemical agents such as betaine, DMSO or formamide that help to prevent the duplex formation. The method may also include modified sequencing reaction conditions that help to relax the problematic structures, like implementing higher temperatures at the denaturation and annealing steps or including a preincubation step during PCR [37].

Sample preparation for this procedure is much more labor intensive as it is recommended to provide linearized plasmids. Therefore, we first digested the pAZ055 ATP11 RNAi plasmid with the NotI restriction enzyme, which cleaves at a single recognition site located outside of our region of sequencing interest. We employed the FastDigest NotI enzyme (Thermo Scientific) and the digestion reaction was setup as shown below (Table 22).

Table 22: NotI restriction mix

Reagent	**Amount**
10x Fast Digest Buffer	8 µl
NotI	5 µl
Plasmid DNA	20 µg
Nuclease-free water	up to 80 µl

After thoroughly mixing the reagents, the reaction was incubated for 2.5 hours at 37 °C. To isolate and concentrate the linearized DNA, the plasmid was precipitated by adding 1/10th volume 3M sodium acetate and 2.5 volumes of 97% ethanol before incubating for 30 minutes in -80 °C. In solution, the sodium acetate dissociates to Na^+ and $[CH_3COO]^-$. The positively charged sodium ions neutralize the negative charge of the PO_3^- groups of the nucleic acids, making the DNA far less hydrophilic and thus much less soluble in water. The ethanol further displaces the H_2O molecules of the DNA solvation shell, leading to precipitation of the DNA in the form of insoluble pellets after centrifugation. Then the DNA is washed with 70% ethanol to eliminate excess salts that may interfere with downstream manipulations. Since this linearized plasmid will also be used in the transfection of *T. brucei*, we need to resuspend the DNA pellet in a sterile environment. Therefore, the sample was transferred to a sterile laminar flow hood, where the ethanol wash was decanted and the DNA pellet was air-dried for 10 minutes. The linearized plasmid was then thoroughly resuspended in 30 µl sterile dH_2O prewarmed to 65 °C. The concentration and purity of the DNA was then measured on the NanoDrop. To verify that the plasmid had indeed been efficiently linearized, we visualized an aliquot of the DNA on an agarose gel. 1 µl of the highly concentrated plasmid DNA was first diluted with 8 µl dH_2O before 1 µl of a 10x DNA dye was added. Then 3 µl of the diluted plasmid was loaded onto an 0.8% agarose gel containing 1 µl ethidium bromide. Included on the gel was a DNA ladder and ~500 ng of uncut plasmid that served as a negative control. The samples were run at 90V for 1.5

hours and then visualized on the Chemidoc. The remaining volume of the linearized plasmid was stored at -20 °C for long term storage until we were ready for *T. brucei* transfections.

We then prepared the reagents for two sequencing reactions, with each designed to sequence through the ATP11 RNAi fragment inserted, either in MCS1 or MCS2. These tubes were comprised of a total of 500 ng of linearized plasmid DNA mixed with 2.5 µl of 10 µM primer. The primers (AZ0461, AZ0462) were selected because they anneal at opposite ends of the LacZ fragment that will form the loop in the hairpin loop RNAi. The opposite orientation of these primers ensure that each sequencing reaction will span one of the two ATP11 RNAi fragments (Figure 17).

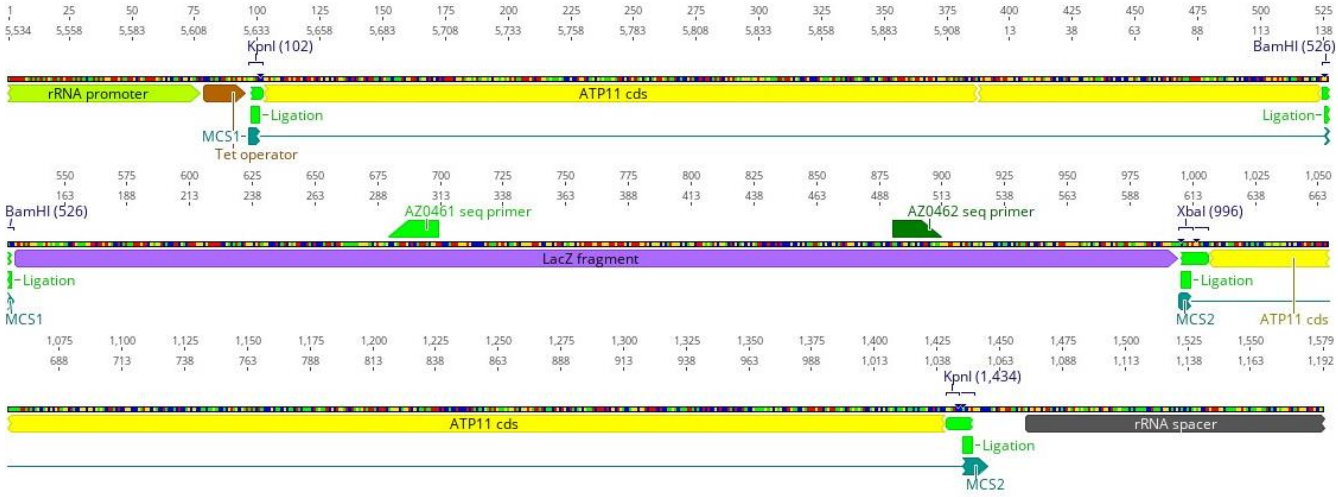

Figure 17: pAZ055 ATP11 RNAi sequencing primers region. ATP11 coding sequence is represented in yellow, while the ligation regions are shown as a light-green blocks underneath. Together these parts represent MCS1 and MCS2, demonstrated as a thin blue line. AZ0461 and AZ0462 stand for forward and reverse sequencing primers respectively (*generated using Geneious*).

Finally, the remaining volume of the prepared sequencing samples was filled with MilliQ water to reach a final volume of 10 µl before they were shipped to SeqMe by mail. After a couple of days, we downloaded the provided ABI chromatographs containing the sequencing results. These were then imported into the software Geneious where they could be aligned with predicted in silico molecules of the pAZ055 ATP11 RNAi plasmid to determine if there were any significant errors.

2.7.8 *T. brucei* transfection

Once the pAZ055 ATP11 RNAi plasmid sequence was confirmed, the linearized DNA with homologous ends to the *T. brucei* rRNA spacer region was ready for transfection. We decided to transfect the PF pSMOX *T. brucei* cell line since procyclic form parasites grow denser in culture, thus limiting the amount of cultures needed for downstream experiments. Furthermore, as discussed earlier, this genetically modified cell line has all the tools needed to generate tetracycline regulated RNAi. Therefore, we thawed and then cultivated a stock of PF pSMOX *T. brucei* for a week to ensure

the culture was healthy with good parasite morphology, movement and doubling time. Next, we needed to prepare the CytoMix transfection buffer (Table 23) used during electroporation, a common method to enhance *T. brucei* uptake of foreign DNA. After that 12 µg of linearized DNA was used for *T. brucei* transfection.

Table 23: CytoMix transfection buffer

Reagent	**[Stock]**	**Volume**	**[Final]**
Hepes, pH 7.6	1 M	2.5 ml	25 mM
KCl	1 M	12 ml	120 mM
$CaCl_2$	1 M	15 µl	0.15 mM
Potassium Phosphate Buffer, pH 7.6	100 mM	10 ml	10 mM
EDTA	0.5 M	400 µl	2 mM
$MgCl_2$	1 M	500 µl	5 mM
Glucose		0.1 g	6 mM
MilliQ H_2O		70 ml	

In order to increase the likelihood that the linearized plasmid will get integrated into the parasite's genome by homologous recombination, we need to make sure that the cell culture is growing in mid-log phase (~0.6 – 1.0 x 10^7 cells/ml). Therefore, 24 hours before the transfection, we split a 10 ml culture to 1x10^6 cells/ml. The next day we harvested a total of 1x10^8 cells, by spinning them in a centrifuge at 1300 xg for 10 minutes at room temperature. After centrifugation, the media was decanted and the *T. brucei* cell pellet was washed with 10 ml of the cytomix buffer. During this centrifugation step, 12 µg of linearized plasmid DNA was loaded into a 0.2 cm gap cuvette. Another cuvette contained the same volume of sterile water as a negative control. Once the centrifugation was completed, the cytomix was thoroughly removed from the cell pellet before it was accurately resuspended in 1 ml cytomix buffer. Then 0.5 ml of the cell suspension was added to the cuvettes and the contents were gently mixed by pipetting up and down. Next, the parasites were electroporated on the exponential decay wave electroporation system BTX ECM 630 with the following settings: 1600 V, 25 Ω and 50 µF. The delivered voltage and the time constant were recorded. The cells were resuspended in 6 ml SDM-79 media containing 10% FBS and 1 µg/ml puromycin, the selectable marker required to maintain the Tet-repressor and T7 RNA polymerase genes within the parasite genome. The cultures were then incubated overnight and allowed to recover for 16-18 hours.

The following day, we began the process of selecting positive clones from a series of limiting dilutions in a 24-well plate. First, another 6 ml of SDM-79 media was added to the cultures, this time the media also contained a 2x concentration (5 µg/ml) of the selectable antibiotic phleomycin. Then 1.5 ml of fresh SDM-79 medium (10% FBS, 2.5 µg/ml phleomycin, 1 µg/ml puromycin) were aliquoted to all the wells in rows B and C of the plate, while 1.0 ml was added to row D. Next, 2 ml of transfected parasites were added to each well in row A. Then, 0.5 ml of transfected cells were transferred from a well in row A to B. After thoroughly mixing the cell culture, this was repeated all

the way down the column. This method resulted in a 1:3 serial dilution of the cells in each successive row on the plate. The health of the cultures in each well were then monitored closely over the following days. When a well was observed to be full of moving parasites, we would gently split them 1:2 into new wells to provide them with added nutrients and fresh antibiotics. Once the well recovered, the culture could be gradually split 1:3, then 1:5 and finally 1:10 into a new 25cm^2 tissue culture flask. The serial dilutions have been designed so that very few cultures ever come to fruition from the largest dilution in row D. Therefore, we usually select 4-5 healthy cultures from row C, which represent the greatest dilution of the originally transfected cell culture. Thus, the cultures in row C are as close to clonal as we can generate using this method.

3. Results

3.1 Growth curves

To determine if the F_1-ATP synthase assembly factors ATP11 and ATP12 perform an essential function in PF *T. brucei* cultivated in SDM-79, we analyzed the growth rate of both uninduced and tetracycline induced RNAi cell lines. In order to maintain the cell cultures at mid-log growth rates, we measured the cell density daily and diluted the cultures with fresh medium accordingly. After collecting data for 9 consecutive days, the cumulative density of each cell culture was calculated and plotted (Figure 18).

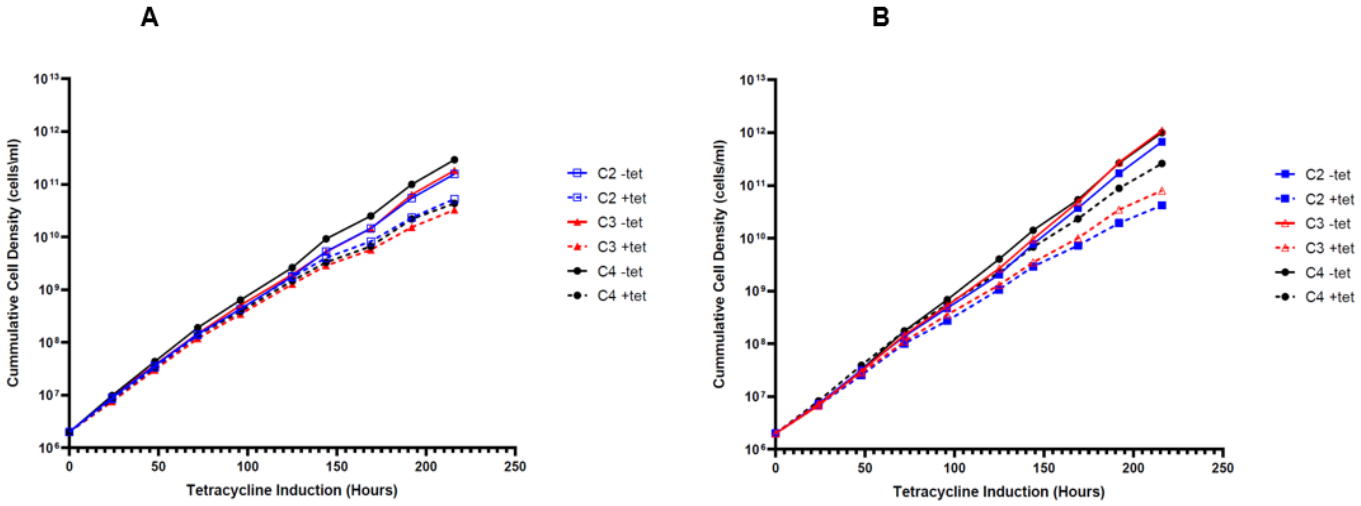

Figure 18: Growth effect on PF pSMOX *T. brucei* depleted of A) ATP11 and B) ATP12 by RNAi. Uninduced cultures are depicted with a solid line, while tetracycline induced cells are illustrated with a dashed line. Three clonal cell lines were included in the analysis, with the uninduced and induced plots color coded.

These graphs indicate that there are mild to intermediate growth defects when ATP11 or ATP12 are depleted by RNAi. These results appear to be fairly reproducible between all three clones of each RNAi. Expectedly, the growth phenotype was not overly dramatic, as the cells were grown in a glucose rich medium and thus were not completely dependent on ATP synthase for ATP production. Therefore, even this intermediate growth effect suggests that the function of these two assembly factors will be essential when the parasites are grown in a more physiologically relevant medium. While both cell lines began their growth defect after day 5 of tetracycline induction, it is apparent that the doubling time is more significantly affected in the ATP12 RNAi cultures (Figure 19). Since clone 3 of each RNAi cell line displayed the most severe growth effects, these two cell lines were chosen to be further characterized.

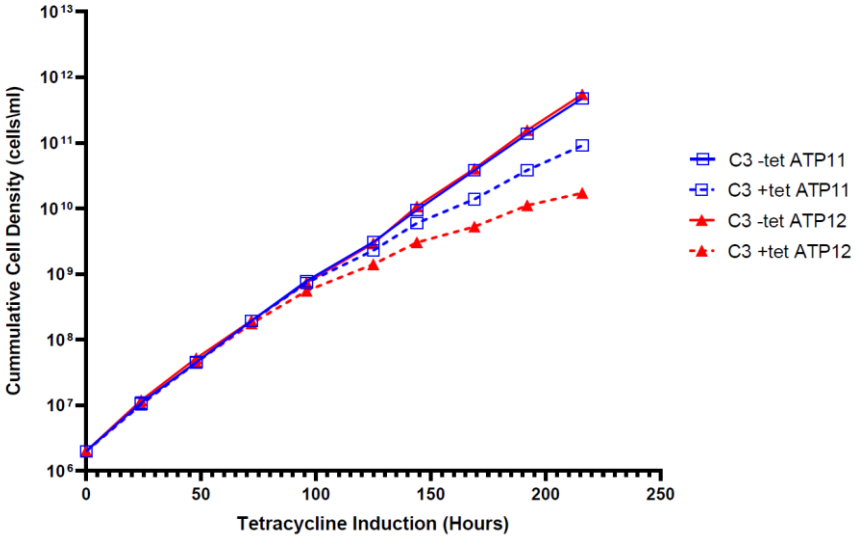

Figure 19: Comparison between the growth effect observed for the PF pSMOX *T. brucei* C3 clones depleted of ATP11 or ATP12 by RNAi. To verify the results from the previous screen, the cumulative density was calculated again from cultures that were RNAi induced a second time. The two RNAi cell lines are again color coded, with the tetracycline induced culture depicted with a dashed line.

3.2 qPCR verification of the RNAi targeted transcripts

Since we lack antibodies raised against *T. brucei* ATP11 or ATP12, we performed a qPCR analysis to calculate how much the targeted transcripts were depleted by RNAi. By isolating the RNA from clone 3 of each RNAi cell line, we measured the relative abundance of a specific transcript by comparing the data from samples induced for 2 or 4 days of RNAi with non-induced samples. These values were normalized to two internal reference housekeeping genes – 18S rRNA and β-tubulin. The ratio of induced/non-induced abundance was then calculated for each induction time point and reference gene separately (Figure 20). A value of 1 indicates no change in the abundance of a transcript, while any value less than 1 depicts a decrease in the transcript stability.

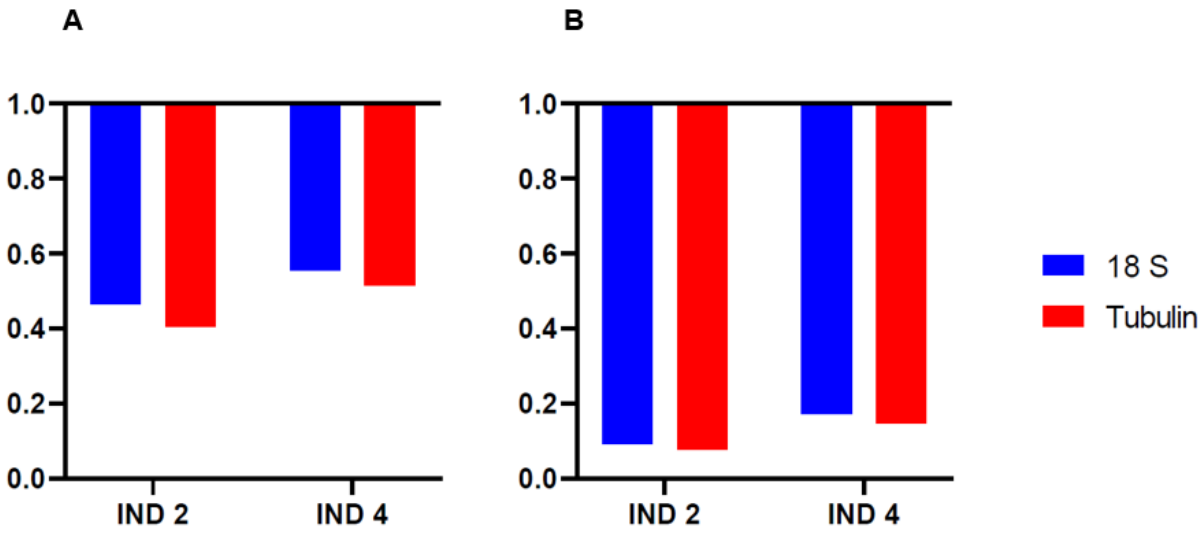

Figure 20: Real-time PCR analysis of A) PF *T. brucei* ATP11 RNAi and B) PF *T. brucei* ATP12 RNAi.

The results revealed a more effective ATP12 knockdown compared to ATP11. This corresponds with the growth curve data for these two cell lines in Figure 19. The milder growth phenotype observed for ATP11 RNAi is likely due to a less efficient RNAi cell line. Therefore, the function of ATP11 is probably just as important as ATP12.

3.3 Steady-state western blot analyses

Since ATP11 and ATP12 are F_1-ATP synthase assembly factors, we wanted to take a quick look at how the stability of the F_1 subunits were affected by the depletion of ATP11 or ATP12. Therefore, whole cell lysates from cultures that were either noninduced or induced with tetracycline were resolved on a denaturing polyacrylamide gel. The proteins were then transferred to a membrane and probed with the primary antibodies at the dilutions indicated below (Figure 21, 23). Each immunoblot was also probed with an antibody that detects the abundant mitochondrial heat shock protein, mtHSP70, which acts as a loading control. From this data, we used scanning densitometry to quantify the intensity of each band (Figure 22, 24).

Figure 21: ATP11 RNAi Western Blot. The equivalent of $1x10^7$ whole cell lysates from ATP11 RNAi cell cultures that were either noninduced (NON) or induced with tetracycline for 2 (IND2), 4 (IND4) or 6 (IND6) days were resolved on a 4-20% polyacrylamide gel. The proteins were then transferred to a membrane and probed with the following primary antibodies at the indicated dilutions: A) α N-term (1:1000 dilution), B) α C-term (1:100 dilution), C) β (1:5000 dilution), D) p18 (1:2000 dilution), E) OSCP (1:2000 dilution) and F) Tb2 (1:2000 dilution). The mtHSP70 blots (1:5000 dilution), acted as a loading control, corresponding to each of the A-F protein.

While the blots represent preliminary data that needs to be optimized further, especially for more accurate and consistent quantification, there are several important outcomes. The ATP11 knockdown data indicates that the expression levels both components of the ATP-synthase peripheral stalk, OSCP and Tb2, are largely unaffected until perhaps day 6 of the RNAi induction. This delayed phenotype is expected because the peripheral stalk forms independently and only interacts with the

F_1-ATP synthase at the latter stages of assembly. However, it is obvious that both the C-terminal and N-terminal subunit α are significantly destabilized by day 4. The data for subunit β is harder to interpret. If we assume that something is amiss with the induced day 4 sample, then it does not appear that the expression levels are affected nearly as much as subunit α, even though ATP11 interacts with subunit β in yeast. Even more striking is that the expression levels of p18 remain unchanged throughout the RNAi time course.

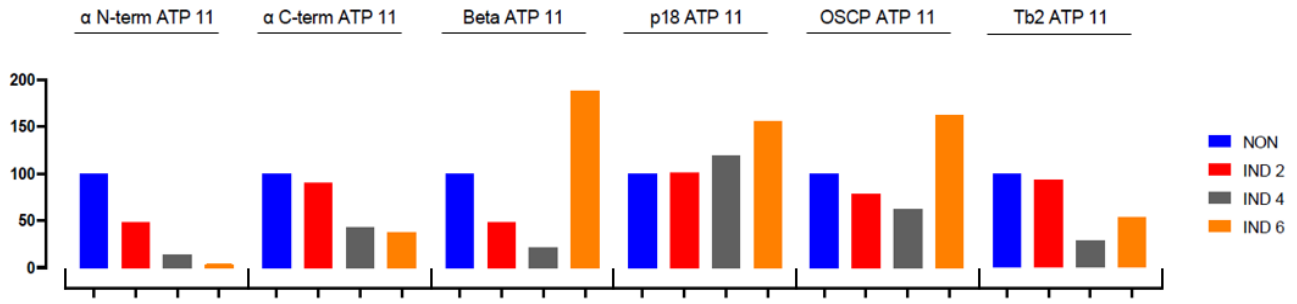

Figure 22: ATP11 RNAi WB quantification analysis. After visualizing the blots from the Western Blot experiment on the ChemiDoc MP Imaging System the intensity of each blot was measured and quantified using the ImageLab software. Each of the protein blot was normalized accordingly to the intensity of the blots from the loading control (mtHSP70).

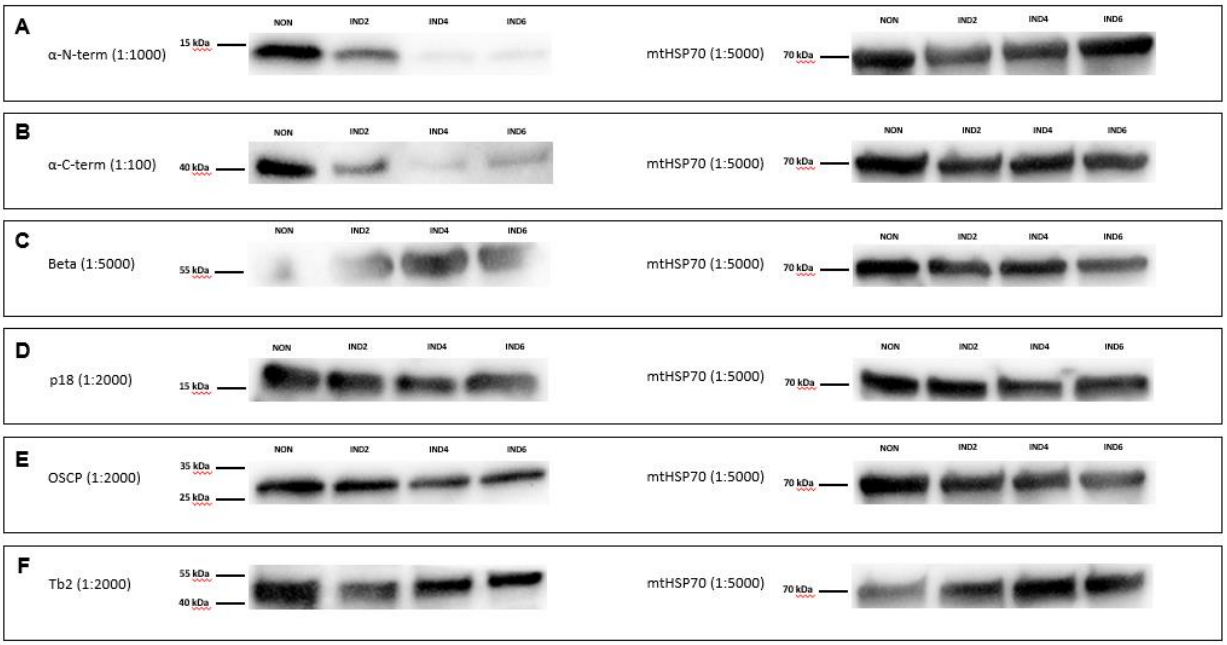

Figure 23: ATP12 Western Blot RNAi. The equivalent of $1x10^7$ whole cell lysates from ATP12 RNAi cell cultures that were either noninduced (NON) or induced with tetracycline for 2 (IND2), 4 (IND4) or 6 (IND6) days were resolved on a 4-20% polyacrylamide gel. The proteins were then transferred to a membrane and probed with the following primary antibodies at the indicated dilutions: A) α N-term (1:1000 dilution), B) α C-term (1:100 dilution), C) β (1:5000 dilution), D) p18 (1:2000 dilution), E) OSCP (1:2000 dilution) and F) Tb2 (1:2000 dilution). The mtHSP70 blots (1:5000 dilution), acted as a loading control, corresponding to each of the A-F protein.

A similar pattern was observed when the ATP12 chaperon was depleted. Again, the amount of the OSCP and Tb2 remained mostly unaltered. As for the F_1-subunits, the abundance of C-terminal and N-terminal subunit α decline considerably. Data for subunit β is unfortunately very hard to interpret again, but it is undoubtedly clear that the expression of p18 protein stays constant.

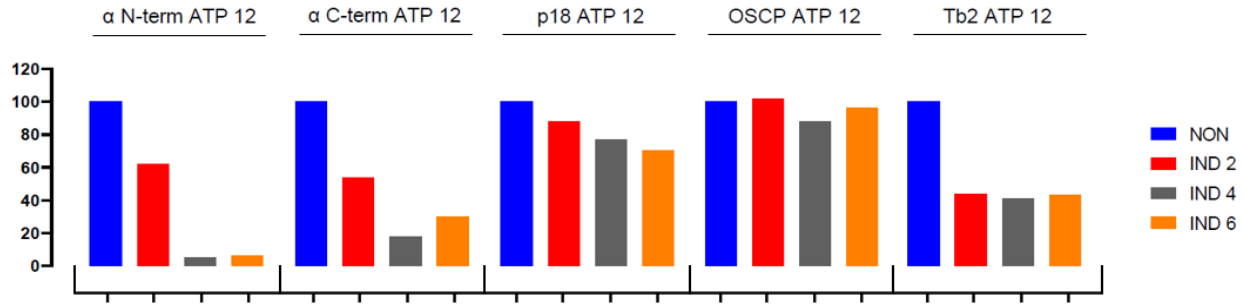

Figure 24: ATP12 RNAi WB quantification analysis. After visualizing the blots from the Western Blot experiment on the ChemiDoc MP Imaging System the intensity of each blot was measured and quantified using the ImageLab software. Each of the protein blot was normalized accordingly to the intensity of the blots from the loading control (mtHSP70).

Overall, the quantity of both C-terminal and N-terminal subunit α peptides are significantly decreased with the disruption of either ATP11 or ATP12, compared to noninduced cells. However, expression levels of the peripheral stalk components, as well as the F_1-ATP synthase subunit p18 remain almost unchanged. As verification of the broad conclusions, we suggest here, a version of this data is repeated again in the following section.

3.4 Blue native western blot analysis

While the steady-state western blots of denatured F_0F_1-ATP synthase subunits give some insights about the loss of F_1-ATP synthase assembly factors, examining the effects of RNAi on the assembly of the entire enzyme would be more fruitful. To determine if the structural stability is altered when ATP11 and ATP12 are depleted, we analyzed protein complexes in their native state. This blue native PAGE method substitutes the denaturing SDS detergent with Coomassie blue to provide a weak charge without disrupting protein folds or protein-protein interactions. To enhance the amount of mitochondrial proteins that can be detected with this method, crude organellar preps are resolved on Bis-Tris polyacrylamide gels before they are transferred to a membrane and probed with the antibodies that recognize F_1-ATP synthase subunits β and p18 (Figure 25A & B). These antibodies detect three major F_1-ATP synthase configurations. The lowest band (~480-720 kDa) depicts the stand alone catalytic F_1-ATP synthase complex, while the middle band (~800-1000 kDa) represents the complete assembled F_0F_1-ATP synthase monomer. Finally, the uppermost band (~1000-1300 kDa) portrays the F_0F_1-ATP synthase dimers.

As a type of loading control, equal amounts of total protein are loaded for each sample. In addition, leftover organellar preps are treated with SDS and analyzed by immunoblotting the denatured proteins (Figure 25C & 9C). The quantification of these denatured bands are much more reliable than measuring the signal intensity detected on blue native PAGE. It is worth noting, that the quality of these denatured gels is much improved here compared to the whole cell lysates analyzed above. Importantly, we observe the same trend as seen previously, where the amount of subunit α is significantly decreased while subunit β and p18 remained unchanged.

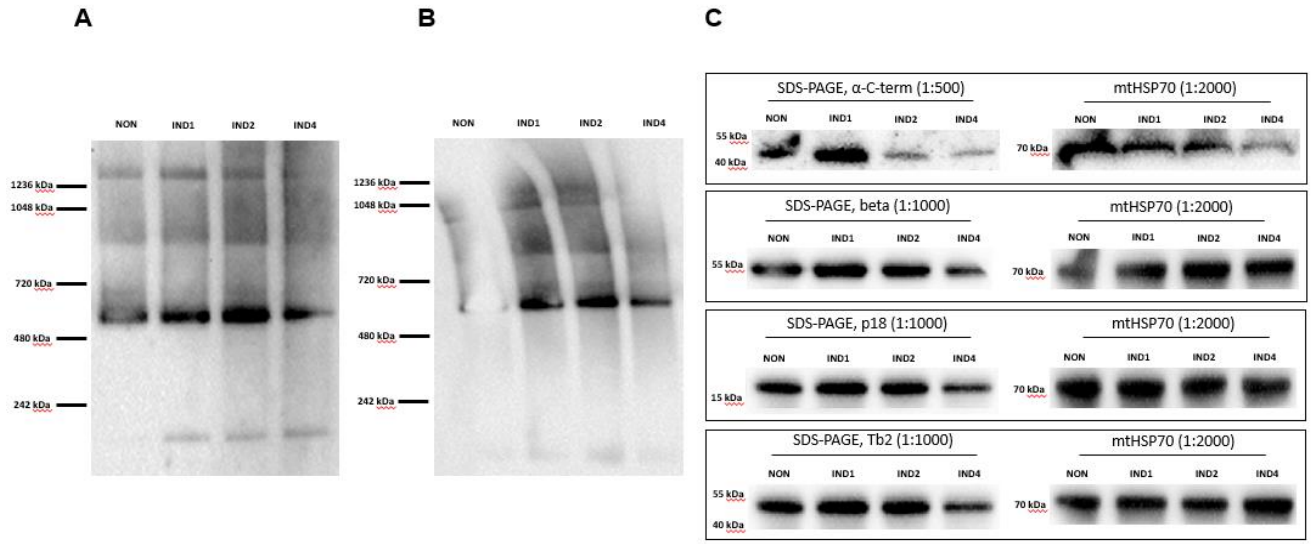

Figure 25: ATP11 RNAi Blue Native Polyacrylamide Gel Electrophoresis. Protein subcomplexes of hypotonically isolated mitochondria from 2,5x10^8 *T. brucei* ATP11 RNAi cell cultures that were either noninduced (NON) or induced with tetracycline for 1 (IND1), 2 (IND2) or 4 (IND4) days were resolved on a 3-12% Bis-Tris gradient polyacrylamide gel. The proteins were then transferred to a membrane and probed with the following primary antibodies at the indicated dilutions: A) p18 (50 µg, 1:1000 dilution), B) β (20 µg, 1:1000 dilution). BN assay loading control C) was done by performing SDS-PAGE, probed with α C-term (1:500 dilution), β (1:1000 dilution), p18 (1:1000 dilution), Tb2 (1:1000 dilution) and corresponding mtHSP70 (1:2000).

Blue native PAGE is often taught as an advanced molecular biology technique because it involves numerous manipulations. While the bands for F_OF_1-ATP synthase monomers and dimers are fuzzy and underrepresented here, the outcomes are representative of the three classic forms of the F_1-ATP synthase. If we focus on the abundance of just the lowest F_1-ATP synthase band, it appears that this structure remains largely unchanged after ATP11 RNAi (Figure 25A & B). In contrast, when ATP12 is depleted, the F_1-ATP synthase structure is drastically destabilized (Figure 26A & B). This significant difference can again be attributed to the lower levels of ATP11 RNAi depletion.

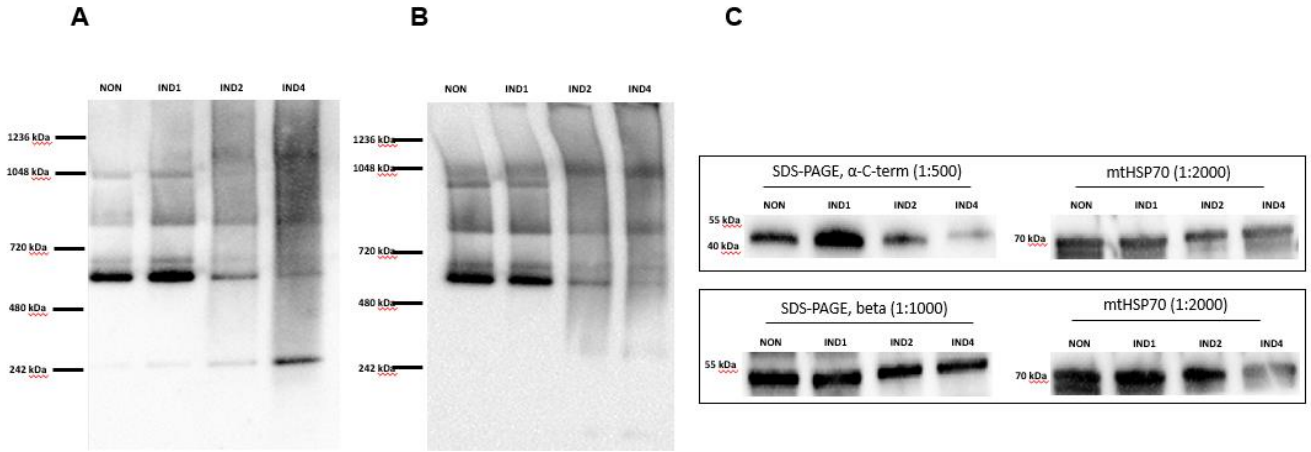

Figure 26: ATP12 RNAi Blue Native Polyacrylamide Gel Electrophoresis. Protein subcomplexes of hypotonically isolated mitochondria from 2,5x10^8 *T. brucei* ATP12 RNAi cell cultures that were either noninduced (NON) or induced with tetracycline for 1 (IND1), 2 (IND2) or 4 (IND4) days were resolved on a 3-12% Bis-Tris gradient polyacrylamide gel. The proteins were then transferred to a membrane and probed with the following primary antibodies at the indicated dilutions: A) p18 (50 µg, 1:1000 dilution), B) β (50 µg, 1:1000 dilution). BN assay loading control C) was done by SDS-PAGE, probed with α C-term (1:500 dilution), β (1:1000 dilution) and corresponding mtHSP70 (1:2000).

Another exciting result from the blue native analyses, is the appearance of subcomplexes comprised of either subunit β or p18. Notably, these lower bands between 100-240 kDa are only detected after ATP11 or ATP12 RNAi is induced. The most prominent of these complexes contains subunit p18, but the mobility of these subcomplexes appears variable depending if ATP11 or ATP12 is depleted. The subunit β subcomplexes appear less sharp and with decreased intensity. Indeed, these subcomplexes are more readily recognizable when its binding partner ATP11 is targeted by RNAi. Furthermore, the subunit β subcomplexes seem to migrate differently from the p18 subcomplexes in both the ATP11 and ATP12 RNAi samples, indicating that there are likely two distinctive subcomplexes formed when these assembly factors are depleted.

3.5 Molecular cloning

Finally, since the qPCR data indicates that the ATP11 RNAi did not deplete the target transcript with nearly the same efficiency as the ATP12 RNAi cell line, we decided to generate a new ATP11 RNAi plasmid that targets a different region of the coding sequence. First, we successfully isolated 3.9 µg/µl of the RNAi plasmid pAZ055 from an *E. coli* glycerol stock. Additional NanoDrop measurements indicated that the sample was sufficiently pure as the ratio of its absorbance at 260 nm and 280 nm was 1.75, which is within the accep

target of 1.8 for DNA samples. Then 10 µg of the plasmid was prepared for the integration of the first ATP11 RNAi fragment by digesting the first multiple cloning site (MSC1) with the pair of restriction enzymes, BamHI and Kpnl. All of the digested plasmid was then resolved on two lanes of an agarose gel to confirm it had been properly linearized (Figure 27) before it was purified from the gel.

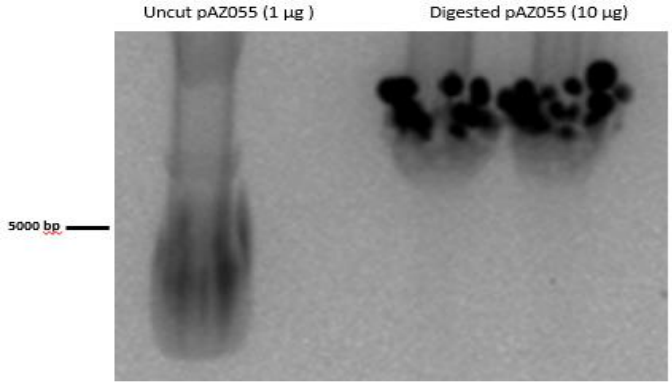

Figure 27: Digested *E.Coli* plasmid DNA pAZ055 using the BamI/Kpn restriction enzymes.

As a control, 1 µg of undigested plasmid was run alongside the digested plasmid. Circular DNA can undertake three different physical conformations that produce three different sized bands when resolved on an agarose gel. The native plasmid DNA conformation found *in vivo* is usually the

supercoiled form, caused by multiple extra twists that make the circular DNA roll up into a tight ball. During replication, the cell needs to access the compacted DNA, so it introduces a single nick in one strand. This relaxes the molecule, relieving most of the twists found in the supercoiled conformation. Finally, the plasmid can be linearized by contaminating nucleases, in which case it migrates based on the length of the DNA. These long linear molecules take more time to navigate through the pores of the agarose gel. Figure 27 indicates that the quality of our plasmid prep was quite good as the molecule exists predominantly in the supercoiled conformation that migrates the fastest through the gel. There is a fuzzy band higher in the gel that indicates some nicked plasmid, which is a common feature. The digested pAZ055 migrates as a single band above 5000 bp, which is consistent with the size of the linearized plasmid. Importantly, the digested plasmid migrated to a different position in the gel than any of the bands in the untreated plasmid DNA. The digested plasmid band appears blurry and splotched because all 10 µg of the digested DNA needed to be isolated from any uncut plasmid in case the digest was not complete. Any undigested plasmid contaminating our linearized plasmid prep would preferentially be taken up by bacteria in the downstream transformations, thus making our cloning efforts very difficult. After the gel extraction, the isolated linearized plasmid was determined to be 154 ng/µl, with an A_{260}/A_{280} ratio of 1.92.

Next, we prepared the new ATP11 RNAi amplicon that will be inserted into the MCS1 of the prepared pAZ055 plasmid above. Based on the GC content of the primers, we chose an annealing temperature of 52 ºC for the PCR reaction. If this parameter is not ideal, the PCR may generate multiple nonspecific bands from the genomic DNA template or it may be very inefficient at amplifying the target molecule. Therefore, we ran the entire PCR reaction on a 1% agarose gel to visualize the DNA molecules amplified (Figure 28). The PCR reaction was quite efficient, producing a predominant band at the expected size of 454 bp. The lower fuzzy band is the result of primer dimers formed during the PCR reaction. It is important to isolate our desired PCR product from these small molecules because they will preferentially ligate into the digested plasmid due to their comparatively higher molarity than our longer PCR product.

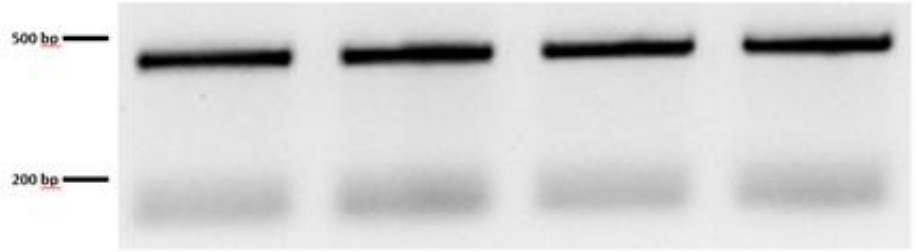

Figure 28: ATP11 RNAi PCR amplicons resolved on a 1% agarose gel. A PCR reaction with 100 ng of isolated *T. brucei* genomic DNA was used as a template for the RNAi primers to anneal and amplify the specific ATP11 454 bp product.

After gel extraction, the ATP RNAi amplicons were measured at 21.2 ng/µl, with an A_{260}/A_{280} of 2.29. While the yield was quite good for this gel extraction kit, the A_{260}/A_{280} ratio above 2.0 indicates that there may be some impurities in our isolated PCR products. This might cause some minor problems during the downstream cloning steps. Next, the amplicons were digested with BamHI and KpnI to produce sticky ends compatible with the digested pAZ055 plasmid. This restriction reaction was then purified with the GenElute PCR clean-up kit (Sigma). At this point, our digested amplicons had a concentration of 17.9 ng/µl and a much better A_{260}/A_{280} of 1.79.

The obtained amplicons were ligated to the linearized pAZ055 plasmid by incubating the DNA with T4 DNA ligase (Table 24). We also prepared one ligation that omitted the amplicon insert, which would serve as a negative control when we performed bacterial transformations with XL-1 *E. coli*. Since no colonies appeared on the negative control plate, it indicated that our linearized plasmid preparations did not contain any uncut plasmid due to an incomplete digestion.

Table 24: Components for pAZ055 plasmid and ATP11 RNAi PCR amplicons ligation

Reagent	**Volume**	**Molarity**
10x Ligation Buffer	1 µl	
DNA vector (154 ng/µl)	1 µl	93.5 µM
DNA insert (17.9 ng/µl)	2.3 µl	121.3 µM
Ligase	1 µl	
MilliQ H_2O	up to 10 µl	

On the other hand, we observed hundreds of colonies on the agar plate containing bacteria transformed with the ligated pAZ055 ATP11 MCS1 plasmid. Due to the negative control, presumably most of these colonies should contain the correct RNAi plasmid. Therefore, we isolated plasmid DNA (Table 25) from just four selected colonies to screen for the proper plasmid. These DNA molecules were analyzed by digesting with the BamHI & Kpnl restriction enzymes and resolving the resulting DNA fragments on an agarose gel (Figure 29).

Table 25: NanoDrop results for the isolated recombinant pAZ055 plasmids

	I	**II**	**III**	**IV**
Concentration	173.3 ng/µl	156.4 ng/µl	107.5 ng/µl	235.9 ng/µl
260/280 nm	1.84	1.87	1.79	1.87
260/230 nm	2.90	3.27	3.95	2.98

Each of the colonies produced the expected DNA fragments, consisting of the smaller ATP11 RNAi insert (432 bp) and the larger pAZ055 plasmid backbone of 5067 bp. Since plasmid DNA from

the 4th colony had the highest concentration and a good A_{260}/A_{280} ratio, it was chosen for further cloning manipulations.

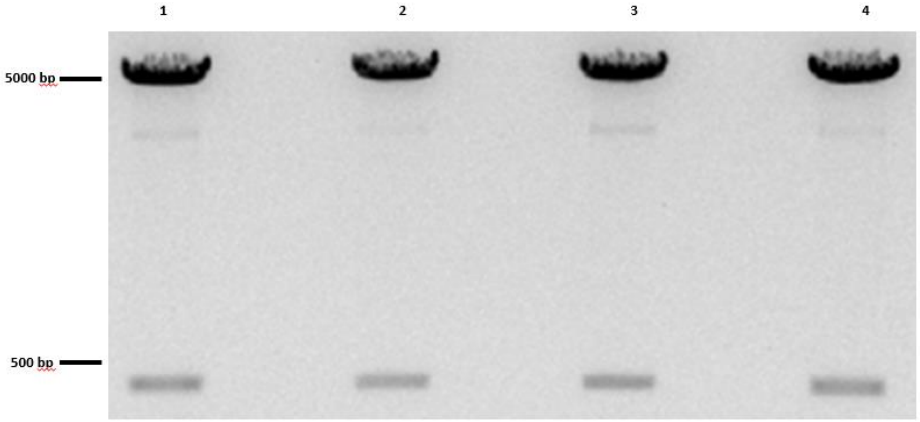

Figure 29: Isolated pAZ055 plasmids (1µg) from four bacterial colonies were analyzed by restriction digest with KpnI & BamHI and then resolved on a 0.8% agarose gel. The expected ATP11 RNAi insert was detected as a band of 432 bp, while the pAZ055 backbone migrated above 5000 bp as predicted.

To finish generating the pAZ055 ATP11 stem-loop RNAi vector, a second ATP11 RNAi amplicon was inserted into the second cloning site using the restriction enzymes XbaI and XhoI. This process followed the same steps as outlined above. The linearization of pAZ055 ATP11 MCS1 clone 4 revealed an intense band at the expected size without the potential traces of any uncut plasmid (Figure 30). After gel extraction, the linearized plasmid had a concentration of 191.5 ng/µl, with an A_{260}/A_{280} of 1.78. Meanwhile, the purification of the digested ATP11 RNAi amplicons resulted in a concentration of 16.6 ng/µl, with an A_{260}/A_{280} of 1.68.

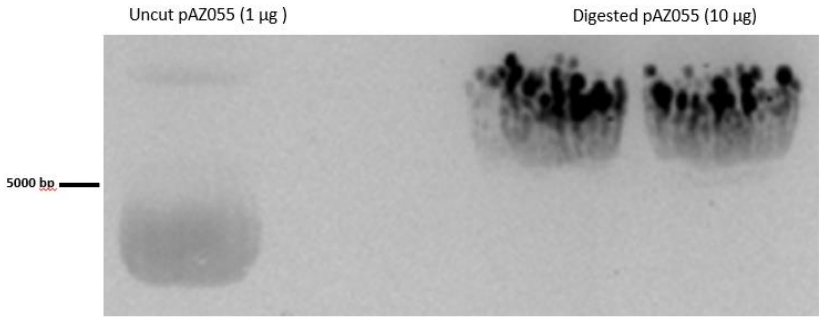

Figure 30: Digested *E.Coli* plasmid pAZ055 using the Xho/Xba restriction enzymes.

The digested plasmid and ATP11 RNAi amplicon were ligated as described before (Table 26). Again, there were no colonies observed on the agar plate incubated with XL-1 *E. coli* cells transformed with the negative ligation control lacking the ATP11 RNAi insert. In contrast, numerous colonies were observed on the plate with bacteria transformed with the entire pAZ055 ATP11 RNAi plasmid. Four clones were selected for plasmid isolation (Table 27).

Table 26: Components for pAZ055 plasmid ligation with complete ATP11 RNAi PCR amplicons

Reagent	Volume	Molarity
10x Ligation Buffer	1 µl	
DNA vector (191.5 ng/µl)	1 µl	116.3 µM
DNA insert (16.6 ng/µl)	3 µl	115 µM
Ligase	1 µl	
MilliQ H_2O	up to 10 µl	

Table 27: NanoDrop results for the isolated pAZ055 ATP11 RNAi plasmids

	I	II	III	IV
Concentration	251 ng/µl	325.6 ng/µl	351.3 ng/µl	278.7 ng/µl
260/280 nm	1.95	1.86	1.89	1.86
260/230 nm	2.31	2.12	2.29	2.16

1 µg of the resulting plasmids were then digested with both sets of restriction enzymes used for cloning into each MCS. The visualization of the digested DNA plasmids indicates that all, except clone 3 digested with BamHI and KpnI, produced bands of the expected sizes (Figure 31). This irregularity in clone 3 eliminated it from our screen of possible plasmids. Interestingly, a closely spaced doublet can be observed for each of the clones digested with BamHI and KpnI. This is entirely expected as both ATP11 RNAi amplicons inserted at MCS1 and MCS2 retained these restriction sites. Using features of the software Geneious, this digest was predicted to produce DNA fragments of 4592 bp for the plasmid backbone, 480 bp for the LacZ fragment and two 432 bp bands for each ATP11 RNAi insert. Importantly, all plasmid clones analyzed with the XbaI & XhoI restriction enzymes produced the expected DNA fragments (444 bp insert and 5484 bp plasmid backbone), revealing the successful incorporation of the ATP11 RNAi amplicon into MCS2. Since clone 2 had the highest plasmid yield (325.6 ng/µl) of the positive clones, it was selected for sequencing and *T. brucei* transfections.

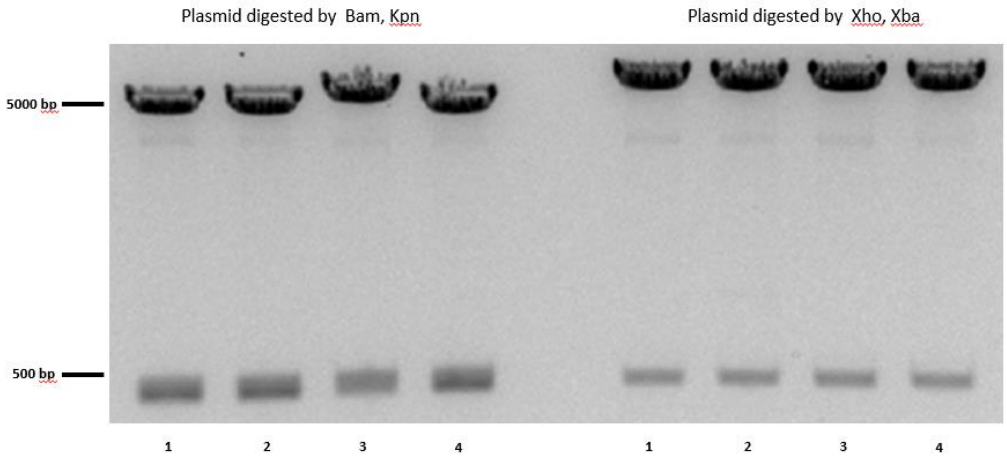

Figure 31: The final pAZ055 ATP11 stem-loop RNAi plasmids were analyzed by restriction digest. Plasmid DNA was isolated from 4 bacterial colonies and then 1 µg of plasmid was digested with either BamI/ and Kpn or with Xho/Xba. The resulting DNA fragments were resolved on a 0.8% agarose gel containing ethidium bromide.

To verify that the pAZ055 ATP11 RNAi plasmid was correct, it was sent for sequencing. Since it contains a hairpin-loop DNA construct, the plasmid needed to be first linearized. Conveniently, there is a single NotI recognition site located outside of the region we would like to sequence. In fact, the NotI linearization of the plasmid generates 5' and 3' ends that can undergo homologous recombination with the *T. brucei* rRNA spacer region. Therefore, we performed a midiprep to isolate a larger amount of this plasmid from the replica plate containing bacterial clone 2. The isolated plasmid had a concentration of 337.6 ng/µl, with an A_{260}/A_{280} of 1.88. 20 µg of the plasmid was digested with NotI, precipitated, washed and then resuspended in sterile water. The resulting plasmid had a concentration of 441.9 ng/µl, with an A_{260}/A_{280} of 1.68. A portion of this linearized plasmid (~1 µg) was then resolved on a 0.8% agarose gel to confirm effective digestion (Figure 32).

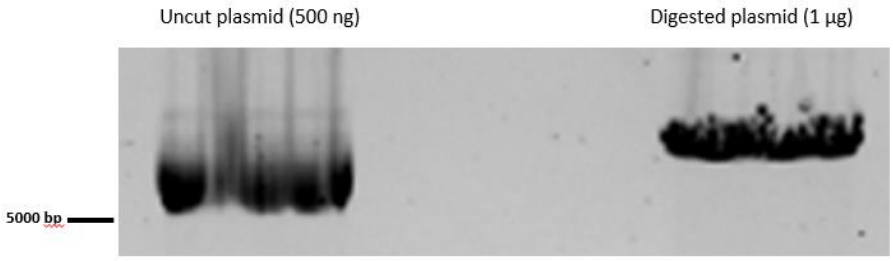

Figure 32: NotI digested pAZ055 ATP11 RNAi clone 2. 1 µg of the linearized plasmid used for sequencing and *T. brucei* transfections was resolved on a 0.8% agarose gel. As a control, 500 ng of the untreated plasmid was also included.

Another portion of the linearized plasmid DNA was submitted for sequencing. The resulting chromatograms were then aligned with the predicted *in silico* sequences (Figures 33, 34). These alignments demonstrated that the pAZ055 ATP11 RNAi plasmid was successfully constructed.

Figure 33: Geneious pAZ0055 ATP11 RNAi sequencing alignment demonstrates the successful integration of the forward ATP11 sequence in MCS1, with the beginning of the sequencing starting from the AZ0461 seq primer. The consensus sequence is indicated at the top with a green bar underneath each nucleotide when there is 100% agreement in the alignment. The bases are color coded: T – red, A – green, G – black and C – blue (*generated using Geneious*).

Figure 34: Geneious pAZ0055 ATP11 RNAi sequencing alignment demonstrates the successful integration of the reverse ATP11 sequence in MCS2, with the beginning of the sequencing starting from the AZ0462 seq primer. The consensus sequence is indicated at the top with a green bar underneath each nucleotide when there is 100% agreement in the alignment. The bases are color coded: T – red, A – green, G – black and C – blue (*generated using Geneious*).

With this confirmation, the linearized plasmid was then transfected into the PF pSMOX *T. brucei* cell line. After the positive selection of transfected clones, the growth curves and qPCR analyses were completed by others in the lab (data not shown). As expected, the qPCR analysis quantified a much higher level of ATP11 depletion, similar to the levels that I calculated for the ATP12 RNAi cell line. Due to this more efficient ATP11 RNAi cell line, the observed growth defects in the tetracycline induced cells was also larger, on par with those detected in the ATP12 RNAi cells.

4. Discussion

The unique structure of the *T. brucei* F_1-ATP synthase presents some intriguing questions surrounding the mechanism of assembling this elaborate enzyme. Creating the typical $\alpha_3\beta_3$ catalytic head piece with alternating subunits requires the assembly factors ATP11 and ATP12, which prevent β and α aggregation, respectively [8]. However, the *T. brucei* F_1-ATP synthase contains an additional three copies of subunit p18 that interacts with the C-terminus of subunit α. The role of this protein is not apparent from the structure of the enzyme as it does not seem to be involved in catalysis. Since the interface between subunit α and p18 largely overlaps with that of subunit α and ATP12, it is possible that this *T. brucei* assembly factor not only prevents subunit α aggregation but also promotes subunit α binding to p18. Further complicating the assembly mechanism, subunit α is proteolytically cleaved into an N-terminal and C-terminal peptide, both of which get integrated into the functional enzyme. The role of p18 could possibly replace the function of ATP12, which may have been repurposed to interact with N-terminal α to make sure that both subunit α peptides are assembled into the mature enzyme.

In order to begin deciphering how this complex enzyme is assembled, we started by analyzing what happens to the *T. brucei* F_oF_1-ATP synthase when we deplete the annotated ATP11 and ATP12 assembly factors by RNAi. Expectedly, the knockdown of ATP11 and ATP12 both produced moderate growth defects when grown in SDM-79, a glucose rich medium. This observation was expected as the parasite does not rely exclusively on the F_oF_1-ATP synthase since it can rapidly synthesize ATP through glycolysis. Even the most efficient knockdown of subunit α only approaches cytostatic growth under these conditions. However, once the RNAi cell lines are adapted to SDM-80, a low glucose medium, the parasites become more dependent on the F_oF_1-ATP synthase. Furthermore, the ATP11 and ATP12 RNAi plasmids could be transfected into the blood-stream form stage of the parasite, where the ATPase activity is absolutely essential for maintaining the mitochondrial membrane potential. It is only under these conditions that it can been demonstrated that the assembly factors ATP11 and ATP12 provide a vital function in the parasite [23].

While the observed mild growth effects were predicted, it was curious that the depletion of ATP11 produced a milder growth phenotype than ATP12. Did this indicate that ATP11 function was less important than ATP12 or was the ATP12 gene product simply more effectively depleted? To answer this, we performed a qPCR analysis that revealed the ATP12 transcript was indeed significantly more reduced compared to ATP11. Therefore, the severity of the growth phenotypes corresponds to the efficiency of each RNAi to deplete the target transcript. While the qPCR indicated discrepancies between the RNAi cell lines, the quantification of the targeted transcripts is not always an accurate predictor of protein expression. This is especially relevant for *T. brucei*, an organism that transcribes long polycistronic RNA molecules that need to be further processed. This means that most regulation

of gene expression occurs post-transcriptionally [38]. Therefore, future endeavors on this project will include generating antibodies raised against the purified ATP11 and ATP12 assembly factors.

Meanwhile, to address the disparity in the RNAi efficiencies between the ATP11 and ATP12 cell lines, it is possible that we were unlucky in the ATP11 clone we selected. However, as depicted in Figure 18, we screened multiple clones for growth effects and then selected the most severely affected clone for qPCR analysis. This indicates that it is an intrinsic problem with the region of the ATP11 transcript that we decided to target by RNAi.

Through personal communications with other labs and our own experiences, it has been documented that targeting various regions of a gene's coding sequence can lead to different levels of transcript suppression. The mechanism for such phenomena is still not fully understood, however secondary structures within the target transcript or proteins that bind RNA could possibly interfere with the ability of RNAi to affect specific regions. Indeed, the new ATP11 RNAi cell line I generated targeting a different region of the ATP11 coding sequence was later found by my colleagues to more efficiently deplete ATP11 and produce a more significant growth defect (data not shown). However, while RNAi time points might allow us to find more intermediate stages of F_oF_1-ATP synthase assembly, an alternative strategy would be to completely remove the assembly factors from the genome. This more time consuming process relies on homologous recombination to replace each locus of the gene with a selectable marker [39]. Alternatively, a CRISPR/cas-9 cell line could be used to knockout both alleles at once [40]. Since we anticipate that these gene products will be essential, most likely we will need to incorporate a regulatable ectopic copy of the genes that can rescue the knockout phenotype.

To analyze how the stability of various subunits of the ATP-synthase are affected with the loss of either ATP11 or ATP12 chaperons, we performed Western Blot assays. Despite the common trend that expression levels of subunit α are significantly affected by the loss of either ATP11 or ATP12, the quality of the data need to be improved for more accurate interpretations. Ideally, the whole Western Blot analysis needs to be repeated at least three times in order to have reliable, consistent data. Our assay, unfortunately, was abruptly interrupted by the Covid-19 pandemic. For future studies, we suggest optimizing the amount of protein loaded and the dilutions of the antibodies. Since the antibody dilutions were quite high, we could load much less protein, for instance $3x10^6$ cell equivalents instead of $1x10^7$. This can dramatically increase the resolution of the bands in the gel. Another possible recommendation is to utilize a fluorescent detection method instead of chemiluminescence. Since this technique has a long stability and linearity over a broad range, fluorescent western blotting provides accurate and quantitative results. In addition, the application of secondary antibodies with different colored fluorescence allows for multiple targets to be analyzed on the same blot (multiplexing) [41].

Despite being a technically demanding assay, our Blue Native Western Blot (BN-WB) results are quite acceptable, especially in regard to the F_1-ATP synthase complexes. Notably, the amount of F_1-ATP synthase complexes is drastically depleted in the ATP12 RNAi cell line, while little change is detected in the ATP11 RNAi cell line. This corresponds with our qPCR data that ATP11 expression was not significantly reduced compared to ATP12. The more severe F_1-ATP synthase phenotype in the ATP12 RNAi cell line is a reasonable outcome if *T. brucei* ATP12 interacts with subunit α, like it does in yeast. However, subunit α expression levels are also significantly decreased in the ATP11 RNAi cell line, while subunit β and p18 levels were largely unaffected. It is possible that *T. brucei* subunit α has a shorter half-life than subunit β, making it less stable under stressful conditions. Another interpretation is that subunit α expression levels are in significant excess to what is actually needed for the assembly of all the mitochondrial F_oF_1-ATP synthases. Therefore, the levels of subunit α were probably only reduced enough to affect the stability of the F_1-ATP synthase when its interacting partner ATP12 is depleted. Perhaps, with greater levels of ATP11 RNAi depletion, we would detect a more severe effect on subunit β expression levels and a corresponding decrease of F_1-ATP synthase.

The goal of this experimental design was to identify F_1-ATP synthase subcomplexes that would indicate how the unique *T. brucei* catalytic head group is assembled. Notably, our BN-WB analyses revealed the presence of both p18 and subunit β subcomplexes when either ATP11 or ATP12 were targeted by RNAi. Subcomplexes containing p18 appear more abundant than those for subunit β, but this might be due to the differences in the overall strength of binding between the antibodies and their protein target under native conditions. Furthermore, implementing the new ATP11 RNAi cell line with more robust depletion of ATP11 might increase the abundance of the subunit β subcomplexes under these native conditions. The resolution and signal intensity of the subunit β subcomplexes are more obvious in the ATP11 RNAi cell line, but some are still detected in the digital image of the ATP12 RNAi samples. This would be in contrast to the results described for yeast, where β agglomerates were only detected during ATP11 depletion, which demonstrated their direct interaction [16, 42]. However, our results need to be repeated to verify this result.

Now that we can identify these F_1-ATP synthase subcomplexes, we would like to determine their composition, which could be another potential area for a future research. Interestingly, the p18 subcomplexes are detected at different molecular weights when comparing the ATP11 and ATP12 RNAi samples. Furthermore, the p18 subcomplexes seem to migrate more slowly through the polyacrylamide gel than the subunit β subcomplexes detected in the ATP11 RNAi cell line. However, these discrepancies in size are difficult to interpret since native protein ladders are notoriously hard to resolve and are highly variable from gel to gel due to the nature of the experiment. Additionally, most native protein ladders do not have many lower molecular weight references that would run

around the size of our detected subcomplexes. Therefore, it is necessary to repeat this procedure several more times with additional protein ladders to determine if the observed patterns persist in a consistent manner. Alternatively, the organellar material could also be resolved on a glycerol gradient. In this technique, proteins move through a linear gradient of the viscous glycerol until their buoyancy matches that of their surroundings. This sedimentation co-efficient is then measured in Svedberg (S) units. Basically, heavier things sink in the glycerol gradient, while lighter objects float. The gradient can then be fractionated into smaller parts and these can be analyzed for F_1-ATP synthase proteins by SDS-PAGE western blots probed with antibodies that detect subunits β, p18 and N-terminal and C-terminal α. This might help resolve if the subunit β and p18 subcomplexes overlap or not. If they do not overlap, the composition of these subcomplexes could be identified by submitting these protein glycerol fractions for mass spectrometry.

The proteolysis of subunit α and the addition of p18 would suggest that *T. brucei* will require more than the assembly factors ATP11 and ATP12 to build a proper F_1-ATP synthase. To discover these potential candidates, we can apply a Proximity-dependent Biotin Identification (BioID) technique. BioID enables to examine interactions between physiologically close proteins in living cells, by utilizing a special biotin ligase enzyme. This enzyme is used to categorize proteins based on their proximity in a process called biotinylation. The ligase is firstly bind to the target protein and then is expressed in cells, where it biotinylates relevant endogenous proteins. Since this enzyme has a rare modification in nature, selection and identification of such proteins is then performed by an ordinary biotin-affinity capture [43]. The proteins isolated by this technique could be verified as bona fide assembly factors by depleting their gene products and observing the F_oF_1-ATP synthase phenotypes previously outlined in the thesis. These new genetic tools could perhaps lead to more intermediate assembly complexes that will help solve the mystery of *T. brucei* F_1-ATP synthase assembly.

5. Conclusion

Despite limited access to the laboratory during the early stages of the COVID pandemic, the *T. brucei* ATP11 and ATP12 RNAi cell lines generated some exciting preliminary data about the assembly of this modified F_1-ATP synthase. Since the composition and architecture of this parasitic enzyme is more complex than those first identified in yeast and mammalian cells, there are likely to be additional assembly factors involved in building this near universal rotary machine. The characterization of the ATP11 and ATP12 RNAi cell lines has led to the identification of both p18 and subunit β subcomplexes. Further investigations into these cell lines will provides new insights about the intermediate assembly processes of this early diverging protist.

6. Literature

1. Baker J. R., (1995). The subspecific taxonomy of *Trypanosoma brucei*. *Parasite*. Vol. 2, P. 3-12.
2. Masocha W., Kristensson K., (2012). Passage of parasites across the blood-brain barrier. *Virulence*. Vol. 3, P. 202-212.
3. Huang, G., Vercesi, A., Docampo R., (2013). Essential regulation of cell bioenergetics in *Trypanosoma brucei* by the mitochondrial calcium uniporter. *Nat Commun*. Vol. 4**,** P. 2865
4. Vanderheyden, N., Wong, J., Docampo R., (2000). A pyruvate-proton symport and an H^+-ATPase regulate the intracellular pH of *Trypanosoma brucei* at different stages of its life cycle. *Biochem. J.* Vol. 346, P. 53-62.
5. Tonini M.L., Peña-Diaz P., Haindrich A.C., et al., (2018). Branched late-steps of the cytosolic iron-sulphur cluster assembly machinery of *Trypanosoma brucei*. *PLoS Pathog*. Vol. 14.
6. Coustou V., Besteiro S., Biran M., et al., (2003). ATP generation in the Trypanosoma brucei procyclic form: cytosolic substrate level is essential, but not oxidative phosphorylation. *J. Biol. Chem.* Vol. 278, P. 49625-35.
7. Garrido, C., Galluzzi, L., Brunet, M., et al., (2006). Mechanisms of cytochrome c release from mitochondria. *Cell Death & Differentiation*, Vol. 13, P. 1423-33.
8. Rühle T., Leister D., (2015). Assembly of F_1F_0-ATP synthases. *Biochimica et Biophysica Acta*, Vol. 1847, P. 849-860
9. Weber J., (2006). ATP synthase: subunit-subunit interactions in the stator stalk. *Biochim. Biophys. Acta*. Vol. 1757, P. 1162-70.
10. Moran L., (2007). How Cells Make ATP: ATP Synthase. *Sandwalk*. Web reference: https://sandwalk.blogspot.com/2007/12/how-cells-make-atp-atp-synthase.html
11. Scanlon B., Al-Shawi J. A., Le M. K., et al., (2007). Determination of the Partial Reactions of Rotational Catalysis in F_1-ATPase. *Biochemistry*, Vol. 46, P. 8785-8797.
12. Kresge N., Simoni R., Hill R., (2006). ATP Synthesis and the Binding Change Mechanism: the Work of Paul D. Boyer. *J. Biol. Chem.* Vol. 281, P. 18-20.
13. Ackerman S.H., (2002). Atp11p & Atp12p chaperone F_1 ATPase biogenesis. *Biochim. Biophys. Acta*. Vol. 1555, P. 101-105.
14. He J., Ford C. H., Carroll J., et al., (2018). Assembly of the membrane domain of ATP synthase in human mitochondria. *PNAS*, Vol. 115, P. 2988-2993.
15. Sharon H., Ackerman S.H., Tzagoloff A., (1990). Identification of two nuclear genes (ATP11, ATP12) required for assembly of the yeast F_1-ATPase. *Proc. Natl. Acad. Sci*, Vol. 87, P. 4986-4990.

16. Franco L., Su C. H., Tzagoloff A., (2020). Modular assembly of yeast mitochondrial ATP synthase and cytochrome oxidase. *Biol. Chem*, DOI: 10.1515/hsz-2020-0112
17. Lefebvre-Legendre L., Salin B., Schaeffer J., (2005). Failure to Assemble the $\alpha_3\beta_3$ Subcomplex of the ATP Synthase Leads to Accumulation of the α and β Subunits within Inclusion Bodies and the Loss of Mitochondrial Cristae in *Saccharomyces cerevisiae*. *J. Biol. Chem.* Vol. 280., P. 18386-392.
18. Tzagoloff, A., (1969). Assembly of the mitochondrial membrane system. II. Synthesis of themitochondrial adenosine triphosphatase F_1. *J. Biol. Chem.* Vol. 244, P. 5027-5033.
19. Wang Z., Sheluho D., Gatti D., et al., (2000) The α-subunit of the mitochondrial F_1 ATPase interacts directly with the assembly factor Atp12p. *EMBO.* Vol. 19, P. 1486-93.
20. Ludlam A., Brunzelle J., Pribyl T., et al., (2009). Chaperones of F1-ATPase. *J. Biol. Chem.* Vol. 284, P. 17138-146.
21. Lefebvre-Legendre L., Vaillier J., Benabdelhak H., et al., (2001) Identification of a nuclear gene (FMC1) required for the assembly/stability of yeast mitochondrial F(1)-ATPase in heat stress conditions. *J. Biol. Chem.* Vol. 276, P. 6789-6796.
22. Zeng X., Neupert W., Tzagoloff A., (2007). The Metalloprotease Encoded by ATP23 Has a Dual Function in Processing and Assembly of Subunit 6 of Mitochondrial ATPase. *Mol. Biol. Cell.* Vol. 18, P. 617-626.
23. Zikova, A., Schnaufer, A., Dalley, R.A., et al., (2009). The F(0)F(1)-ATPsynthase complex contains novel subunits and is essential for procyclic *Trypanosoma brucei*. *PLoS Pathog.* Vol. 5.
24. Perez E., Lapaile M., Degand H., et al., (2014). The mitochondrial respiratory chain of the secondary green alga *Euglena gracilis* shares many additional subunits with parasitic *Trypanosomatidae*. *Elsevier.* Vol. 19, P. 338-349.
25. Gahura O., Šubrtová K., Váchová H., et al., (2017). The F1-ATPase from *Trypanosoma brucei* is elaborated by three copies of an additional p18-subunit. *FEBS J.* Vol. 285, P. 614-628
26. Montgomery M.G., Gahura O., Leslie G.W., et al, (2018) ATP-synthase from *Trypanosoma brucei* has an elaborated canonical F_1-domain and conventional catalytic sites. *PNAS.* Vol. 115, P. 2102-2107
27. Yadav K.N., Miranda-Astudillo H.V., Colina-Tenorio L., et. al., (2017) Atypical composition and structure of the mitochondrial dimeric ATP synthase from *Euglena gracilis*. *Elsevier.* Vol. 1858, P. 267-275.
28. Beckman coulter® Z Series *User Manual* 9914591-D
29. Invitrogen. Turbo DNA-free Kit User Guide, *Thermo Fisher Scientific Inc.* Pub. AM1907
30. Pfaffl M. W., (2001). A new mathematical model for relative quantification in real-time RT-PCR. *Nucleic Acids Res.* Vol. 29.

31. Smith, P.K. (1985). Measurement of protein using bicinchoninic acid. *Anal Biochem.* Vol. 150, P. 76-85.
32. Pierce BCA Protein Assay Kit, *Thermo Fisher Scientific Inc.* Pub. 23227
33. Martins-Gomes C., Silva M.A., (2018). Western Blot Methodologies for Analysis of In Vitro Protein Expression Induced by Teratogenic Agents. *Teratogenicity Testing: Methods and Protocols.* Vol. 9, P. 191-203
34. Alsford S., Horn, D. (2008). Single locus targeting constructs for reliable regulated RNAi and transgene expression in Trypanosoma brucei. *Molecular and Biochemical Parasitology,* Vol. 161, P. 76-79
35. GenElute. HP Plasmid Miniprep Kit, *Sigma-Aldrich.* Catalog Nos. NA0150S
36. T4 DNA Ligase, *Promega* Part# 9PIM180
37. Kujanová M., HairpinSeq – a sequencing protocol for difficult templates. *SEQme.* Web-adress: https://www.seqme.eu/en/magazine/HairpinSeq
38. Clayton C., (2019). Regulation of gene expression in trypanosomatids: living with polycistronic transcription. *Open Biol.* Vol. 9.
39. Wirtz E., Leal S., Ochatt C., (1999). A tightly regulated inducible expression system for conditional gene knock-outs and dominant-negative genetics in *Trypanosoma brucei. Elsevier.* Vol. 99, P. 89-101.
40. Soares Medeiros L. C., South L., Peng D., (2017). Rapid, selection-free, high-efficiency genome editing in protozoan parasites using CRISPR-Cas9 ribonucleoproteins. *ASM Journals.* Vol. 8.
41. Eaton, S. L., Roche S.L., Hurtado M. L., et al. (2013) Total protein analysis as a reliable loading control for quantitative fluorescent western blotting. *PLoS One* Vol. 8.
42. Wang Z. G., (2000). The assembly factor Atp11p binds to the beta-subunit of the mitochondrial F1-ATPase, *J. Biol. Chem.* Vol. 275, P. 5767–5772.
43. Roux J. K., Kim D. I., Burke B., et al., (2018). BioID: A Screen for Protein-Protein Interactions. *Curr Protoc Protein Sci.* Vol. 74, P. 1-14.